**Citation (APA)**
Song, G., Voskov, D., Abels, H. A., Vardon, P. J., & Geiger, S. (2026). Data-worth analysis using ensemble smoother with multiple data assimilation to constrain uncertainty in geothermal energy production from clastic fluvial reservoirs. *Computational Geosciences*, *30*(4), Article 53. https://doi.org/10.1007/s10596-026-10460-3

RESEARCH

# Data-worth analysis using ensemble smoother with multiple data assimilation to constrain uncertainty in geothermal energy production from clastic fluvial reservoirs

**Guofeng Song[1] · Denis Voskov[1,2] · Hemmo A. Abels[1] · Philip J. Vardon[1] · Sebastian Geiger[1]**

Received: 22 December 2025 / Accepted: 18 June 2026


**Abstract**
Geothermal energy is a key option for decarbonizing heating and cooling in the energy transition. Forecasting geothermal production has inherent uncertainty due to the heterogeneity of geological formations that host the geothermal resource and the limited data available to characterize and quantify these heterogeneities. This uncertainty leads to operational risks such as early thermal breakthrough. Identifying the most valuable monitoring data and data acquisition strategies for operators is key to constraining uncertainties and ultimately de-risking operations in a reliable and cost-effective way. Data-worth analysis quantifies the value of data provided by existing observations or proposed data collection strategies. This study combines Ensemble Smoother with Multiple Data Assimilation and data-worth analysis to constrain uncertainty in production forecasts and reservoir response for a geothermal doublet system located in a clastic, channelized fluvial reservoir. The main monitoring data includes production temperature, injection pressure, and temperature and pressure profiles along the well paths. We show that production temperature and injection pressure alone only can constrain uncertainties in production forecasts. Using observations of well temperature and pressure profiles demonstrates a threefold increase in data worth, which improves both the quantification of production forecasts and reservoir dynamics. At constant injection rates in doublet system, temperature profiles monitored along the wells provide higher data worth compared to pressure profiles. Data from a deviated monitoring borehole is advantageous. Early-time (first year) observations of temperature and pressure profiles along the injector, producer, and monitoring borehole already constrain production uncertainty prior to thermal breakthrough. Data-worth analysis is shown to be most beneficial when conducted across multiple plausible geological scenarios to ensure a more reliable assessment of collection strategies. The findings of this study yield insight into designing informative data-acquisition strategies for direct-use geothermal systems.

**Keywords** Channelized fluvial reservoir · Geothermal energy production · Data-worth analysis · Ensemble smoother with multiple data assimilation · Uncertainty · Multiple scenarios


https://doi.org/10.1007/s10596-026-10460-3

Published online: 24 June 2026

https://doi.org/10.1007/s10596-026-10460-3

## 1 Introduction

Long-term geothermal energy exploitation is subject to uncertainty due to multi-scale and hierarchical geological heterogeneities, limited knowledge of their spatial distribution, and incomplete conceptual and/or mathematical models of fluid–rock interactions that control flow behavior. These uncertainties affect the assessment of technical and operational risks, such as early thermal breakthroughs, short operational lifespan, or high maintenance costs of installed geothermal systems [1–3].

Data worth has been defined as the extent to which data of a system improves the estimation of model parameters or reduces uncertainty in model predictions [4–6]. Data-worth analysis therefore quantifies the usefulness of data provided by existing observations, proposed data acquisition programs, or prior knowledge about model parameters. From an operational point-of-view, conducting such an analysis early during the appraisal of a geothermal reservoir helps to plan cost-effective data acquisition and monitoring campaigns that ensure resources are focused on characterizing the parameters that are most important to yield reliable reservoir performance forecasts.

Previous studies in data worth have applied both, gradient-based and stochastic approaches, to analyze the worth of data for predictive uncertainty reduction [5, 7]. For example, Finsterle [8] performed local data worth analysis for a 2D homogeneous geothermal reservoir using a sensitivity gradient matrix, and later applied the same method to assess the evolution of a geologic repository for heat-generating nuclear waste [9]. However, data worth estimates depend on the local sensitivity of model predictions with respect to model parameters. For complex reservoir models, nonlinearity and parameter interaction effects further limit the applicability of sensitivity-driven approaches. Stochastic approaches, such as Bayesian data worth analysis, have gained increasing attention in groundwater studies [5, 10–12]. By combining prior information with observations, Bayesian methods produce posterior distributions from which the reduction in predictive or parameter uncertainty can be quantified. Younes et al. [13], for instance, applied Bayesian parameter inference via Markov Chain Monte Carlo (MCMC) for efficient estimation of soil hydraulic properties. Ensemble Kalman filter (EnKF)-based data worth analysis offers an alternative by updating both, model parameters and state variables, sequentially to assess estimation and prediction uncertainty in subsurface flow [4, 10, 14]. Unlike gradient-based methods, ensemble approaches approximate uncertainty from the variance across many ensemble members rather than relying on the Jacobian matrix, which usually refers to the sensitivity of model predictions with respect to model parameters. Nevertheless, in highly nonlinear models, updated state variables (e.g., hydraulic head) and parameters (e.g., hydraulic conductivity) may become inconsistent [15]. To improve efficiency, surrogate models, such as Gaussian process regression [6], polynomial chaos expansion [14], and deep convolution neural networks [16, 17], have been used to accelerate ensemble simulations. Most existing data-worth studies focus on groundwater applications using hydraulic head and solute concentration as primary observations, but relatively few Bayesian data-worth analyses address geothermal production scenarios [7, 18, 19], where temperature and pressure are routinely measured in geothermal systems, mostly at the wellheads, with distributed temperature sensing along wells becoming increasingly common. In contrast, solute concentration measurements obtained from tracer tests incur additional operational costs in geothermal systems.

Data acquisition is frequently linked to decision-making and economic outcomes through the concept of Value of Information (VoI) [20], which extends beyond data-worth analysis by quantifying the economic benefits of information under uncertainty. For example, Barros et al. [21] proposed a comprehensive VoI framework within a closed-loop reservoir management setting, where data assimilation and production optimization are integrated, allowing production strategies to be continuously updated as new information becomes available. Barros et al. [22] further introduced a quantitative model-based framework for $CO_2$ storage conformance verification, demonstrating that pressure measurements alone may provide limited information between subsurface scenarios and may not be sufficient to improve monitoring design. van Wees et al. [23] proposed play-based portfolio VoI for geothermal exploration and applied decision-tree-based approaches combined with Net Present Value (NPV) to evaluate the economic value of information across multiple prospects. They found that the information acquired from early-stage projects can significantly influence subsequent decisions, particularly when geological properties exhibit spatial correlation [24]. These studies highlight that geological uncertainty plays a critical role in subsurface decision-making, and that the real value of information lies in its ability to inform monitoring and development strategies.

Data assimilation is rooted in Bayesian theory, integrating prior equiprobable realizations, forward simulations, and field observations to generate posterior realizations for uncertainty estimation [25]. Ensemble Smoother with Multiple Data Assimilation (ES-MDA) [26] is one method used for data assimilation that has gained increasing popularity in subsurface characterization of properties for geothermal reservoirs, and is particularly effective for weakly nonlinear and high-dimensional problems as they avoid explicit computation of the Jacobian matrix [27–30]. ES-MDA is computationally efficient, flexible, and capable of integrating multi-source data. As an extension of the ensemble smoother, ES-MDA addresses nonlinearity in the model-data relationship by updating ensemble realizations over multiple assimilation steps using observed data. In ES-MDA, model parameters are explicitly updated while state variables are implicitly updated through forward simulation. This approach avoids the potential inconsistencies between parameters and state variables that may arise in EnKF due to joint updates in nonlinear systems. These advantages make ES-MDA a promising foundation for data-worth analysis for geothermal systems, enabling the identification of the most informative temperature and pressure observations for reducing uncertainties and de-risking operations.

Geological uncertainty is mainly related to two factors: first, the reservoir architecture, which refers to the spatial arrangement of major geological features such as facies and channel structures in the subsurface formation. For example, the 3D distribution and connectivity of permeable facies is difficult to characterize; second, there is limited information about the spatial distribution of the petrophysical properties such as porosity and permeability [2, 31–34]. For example, Aghaei et al. [35] showed that geological heterogeneity in meander-belt architectures strongly influences the evolution of the thermal plume and the timing of cold-water breakthrough in geothermal doublets. It is therefore important to develop reservoir models that represent different reservoir architectures because a single reservoir model that is built around a single base case leads to biased predictions that underestimate uncertainties in reservoir performance forecasts and ultimately assesses operational risks insufficiently [4]. Xue et al. [12, 15] proposed multimodal data assimilation that combines EnKF with a Bayesian Model Averaging framework to reduce uncertainty in the reservoir properties and state variables of a groundwater system where multiple geological concepts were considered. The posterior uncertainty for the model ensemble was obtained as the weighted combination of the results from all individual reservoir models. Zhan et al. [19] developed a stochastic deep learning framework for data-worth analysis to identify facies distributions, coupling it with non-isothermal flow and transport simulations. Reservoir facies were parameterized using a GAN (Generative Adversarial Network) and a surrogate model was employed to accelerate predictions of temperature, concentration, and pressure.

This study aims to develop a data-worth analysis framework for geothermal systems while accounting for both, uncertainties in reservoir architecture and petrophysical property distributions; i.e., we consider uncertainties in the geological concepts that define the different geological scenarios for the reservoir architectures as well as the uncertainties in the spatial distribution of permeability and porosity that are modelled using stochastic methods. We use the Delft campus geothermal project (Geothermie Delft) for developing our framework. This geothermal project was established to supply thermal energy to the built environment of the TU Delft campus and parts of the city of Delft while also providing a research infrastructure [36, 37]. The geothermal resources are located in the lower Cretaceous Delft Sandstone Member, a clastic reservoir at 2 km depth in the West Netherlands Basin. The Delft Sandstone Member has been interpreted as stacked, distributary-channel deposits in a lower coastal plain environment, resulting in extensive sandstone sequences intercalated by floodplain fines [36, 38, 39]. The same reservoir unit is already used in multiple geothermal doublet systems in the area, such as in two other projects only 2 to 4 km adjacent to the Delft campus geothermal project. It is well known that it is difficult to forecast the production from geothermal systems located in channelized fluvial reservoirs because of the limited data availability and hence the incomplete understanding of the subsurface geology [40, 41]. To enhance the understanding of the geothermal system behavior and

 https://doi.org/10.1007/s10596-026-10460-3

constrain uncertainties in the reservoir performance forecasts, data acquisition and monitoring strategies need to be designed in a way that they maximize the value of data while minimizing costs. Ultimately, tailored data acquisitions are key to reducing operational risks such as unscheduled downtime or early breakthrough of cold water. In other words, it is important to quantify the data worth, i.e. identify the most valuable data that needs to be collected to ensure that reservoir performance forecasts for geothermal systems are reliable.

In our previous study [42], we developed a scenario-based ES-MDA framework that integrates efficient scenario-based geological modeling via Rapid Reservoir Modelling (RRM) [43, 44], high-fidelity production simulation with the open-source Delft Advanced Research Terra Simulator (open-DARTS) [45], and ES-MDA to explore, quantify, and constrain uncertainties in the channelized fluvial geothermal systems. Multiple reservoir architectures were considered to account for both, different geological scenarios and different petrophysical property distributions, which enabled a more robust approach to quantifying and constraining uncertainties in production forecasts.

Building on this scenario-based data assimilation framework, we now evaluate the data worth of different observation schemes by measuring how much the uncertainty in reservoir response decreases from the prior ensemble to the posterior ensemble. This novel approach integrates flow and heat transfer simulation in fluvial geothermal systems using open-DARTS [45], ES-MDA with different types of observation data, and quantitative data-worth analysis to quantify the value of different data acquisition schemes and data types. We apply this approach to an ensemble of channelized fluvial reservoir models that are inspired by the Delft campus geothermal project. These ensembles consider both, different reservoir architectures and equiprobable stochastic representations of the reservoir properties. First, we perform an uncertainty analysis for this ensemble to characterize production performance and compute the temperature and pressure profiles along the wells, revealing the uncertainty in reservoir performance forecasts in time and space. Next, the data worth is calculated from ES-MDA results for a single reservoir architecture using the following types of data: temperature of the produced fluid, bottom hole pressure at the injection well, and temperature and pressure profiles recorded along the injection and production wells, as well as a monitoring borehole. We then vary the locations of the monitoring boreholes, the monitoring periods, and the combinations of observational data (e.g., temperature of produced water and bottom hole pressure of injection well only or in combination with pressure and temperature profiles recorded along the wells) to identify the data types and acquisition strategies that yield the most value of data for reducing uncertainties in production forecast. Finally, we repeat this data-worth analysis for different reservoir architectures to not only consider the geological uncertainty captured through equiprobably stochastic modelling of the reservoir properties for a single reservoir architecture but to also account for the much broader range of geological uncertainties inherent to different geological scenarios and concepts.

The remainder of this paper is organized as follows: Sect. 2 describes the methodologies for geological modelling, simulating heat and fluid flow in a geothermal system, ES-MDA, and the data-worth analysis. Section 3 presents results for the data-worth analysis when considering different data acquisition strategies, including the analysis for different reservoir architectures. Sections 4 and 5 provide discussion and conclusions, respectively.

## 2 Methodology

Our data-assimilation-based data-worth analysis for quantifying and reducing the uncertainty in performance forecasts for geothermal systems developed in channelized fluvial geothermal reservoirs is based on four key components: (1) creating the ensemble of reservoir models; (2) simulating heat and fluid flow in the reservoir; (3) applying the ensemble smoother with multiple data assimilation across equiprobable realizations to constrain uncertainties in production and reservoir response with different data types and amounts; and (4) evaluating data worth based on the assimilation results.

### 2.1 Geological model and model set-up

Channelized fluvial reservoir models are created using the Delft campus geothermal project as inspiration. That is, the models capture some of the key uncertainties inherent to the reservoir that hosts the Delft campus geothermal project but the models are still generic enough such that learnings can be transferred to other geothermal projects hosted in channelized fluvial systems. A key simplification is that the reservoir is assumed to contain only sandstone and mudstone facies, representing the main channel and floodplain, respectively. The geothermal doublet in this study comprises a vertical production well and a vertical injection well that both fully penetrate the reservoir model (Fig. 1). A monitoring borehole is also considered, located equidistant in between the two wells. This borehole also penetrates the entire reservoir model. Such a borehole is planned for the Delft campus geothermal project as part of the EPOS-eNLarge project (https://epos-nl.nl/enlarge/). Note that the presence of a monitoring borehole is a rare exception because the Delft campus geothermal project also has a strong research component, in addition to providing the campus and part of the city with heat. For most direct-use geothermal projects, monitoring boreholes are not drilled due to budget constraints and the high drilling costs. We also define four virtual lines that penetrate the full reservoir model and record pressure and temperature along these lines during the simulations, which yields additional information for the data-worth analysis and allows us to quantify how such data impacts uncertainty quantification. The lines are placed symmetrically around the monitoring borehole at equal distance.

Figure 1 presents the facies and the porosity and permeability distributions of a geological model that provides the reference solution for this study, i.e. we regard this model as the reference (or ‘truth’) and exclude it from the ensemble so that simulation results from the ensemble can be compared to the reference solution. The facies model is generated through a modified Rapid Reservoir Modelling (RRM) approach in which channelized fluvial layers are randomly selected from a library and stacked with overlaps to ensure that there can be vertical connectivity in sand channels. As noted above, the model contains two facies: sandstone, representing channel belts, and mudstone, representing floodplain deposits. The porosity and permeability are assumed to be heterogeneous in sandstone and constant in mudstone because the flow rates are negligibly low in the mudstone facies. Porosity distributions in the sandstone facies were generated using Sequential Gaussian Simulation (SGS). Details of the SGS algorithm and parameter settings are provided in [46, 47]. Using the porosity–permeability relationship

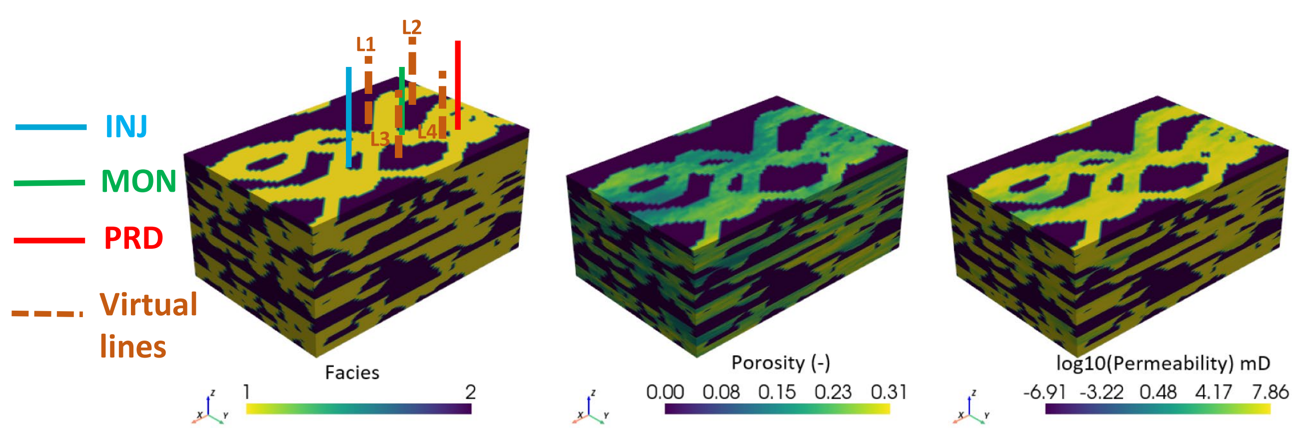


**Fig. 1** Schematic of a model of a channelized fluvial geothermal reservoir showing two facies (1: sandstone, 2: mudstone) with their porosity and permeability distributions, as well as the locations of the injector (INJ), producer (PRD), monitoring borehole (MON), and four virtual lines (L1, L2, L3, and L4) for collecting additional data during the simulations. Data-worth metrics are calculated along the L1, L2, L3, and L4. These lines allow us to quantify the effects of the number and locations of monitoring boreholes on data worth. The model shown here is the reference model that provides reference data based for the data assimilation framework

derived from core analysis at well GT-02 from the Delft campus geothermal project [37, 38], permeability is calculated for each realization as.

$$\begin{aligned}\log_{10}(k) = &-3.523 \cdot 10^{-7} \cdot \varphi^5 + 4.278 \cdot 10^{-5} \cdot \varphi^4 - 1.723 \cdot 10^{-3} \cdot \varphi^3 \\ &+1.896 \cdot 10^{-2} \cdot \varphi^2 + 0.333 \cdot \varphi - 3.222\end{aligned} \tag{1}$$

100 equiprobable stochastic realizations with different porosity and permeability distributions were generated for the reference geological scenario (i.e. reference reservoir architecture) by using SGS. Four example realizations from the ensemble of porosity–permeability models for reference architecture are presented in Fig. 2.

In reality, the true subsurface reservoir architecture, particularly the spatial distribution of fluvial channel bodies and their connectivity, is unknown. As noted before, it is well understood that uncertainty quantification methods that rely only on a single reservoir architecture lead to a biased assessment of reservoir uncertainties and performance forecasts. It is therefore necessary to evaluate data-worth analysis for different reservoir architectures. We hence employ a scenario-based geological modeling approach to generate 10 further geological scenarios [42, 44]. Five scenarios are constrained by the facies distributions along injection and production wells, and the other five are generated without any facies constraints. The reference facies distribution is that of the reference scenario. Figure 3 shows the reference geological scenario together with two additional scenarios, one with the facies constrained to the well logs and the the other without such constraints. From each geological scenario, 100 equiprobable stochastic realizations of porosity and permeability are generated, yielding 10 different reservoir model ensembles and 1,000 geologically diverse reservoir models in total.

## 2.2 Forward modeling

Reservoir simulation of low-enthalpy geothermal systems, such as the Delft campus geothermal project, is based on the standard mass and energy conservation equations for slightly compressible single-phase flow

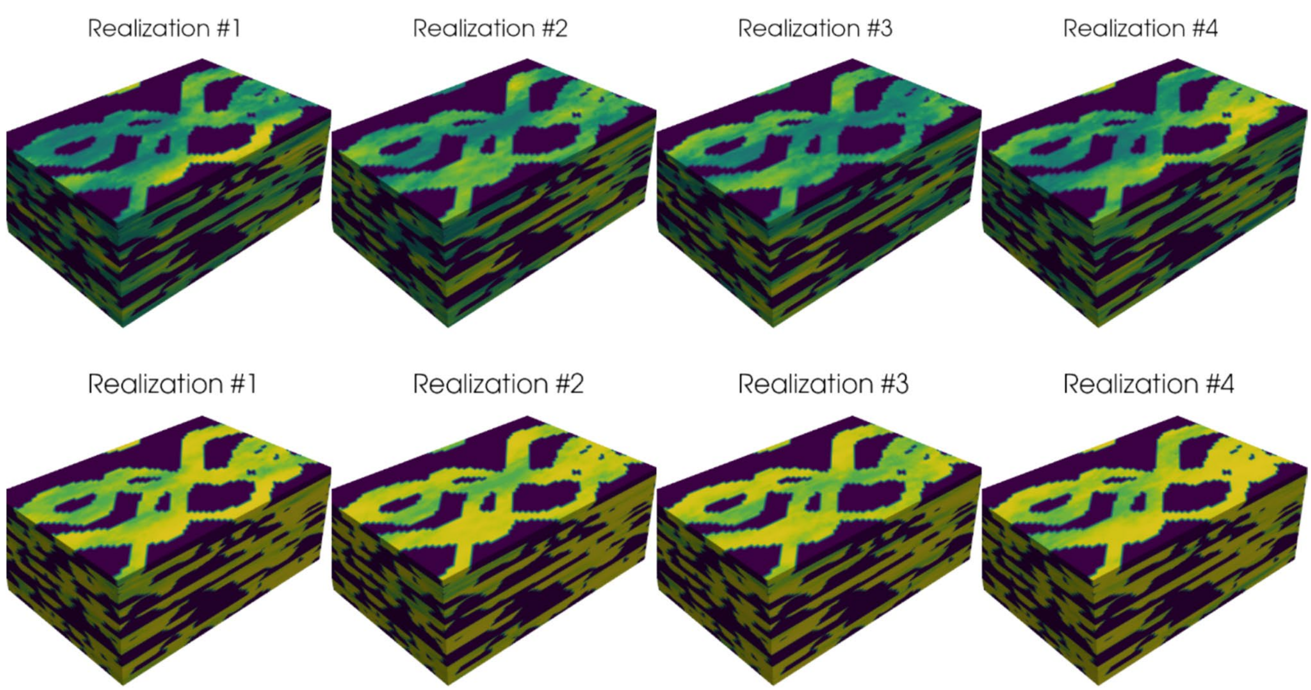


**Fig. 2** Four example porosity–permeability realizations of the reference reservoir architecture illustrating the different porosity (upper) and permeability (lower) distributions. The color bars for porosity and permeability are the same as those in Fig. 1

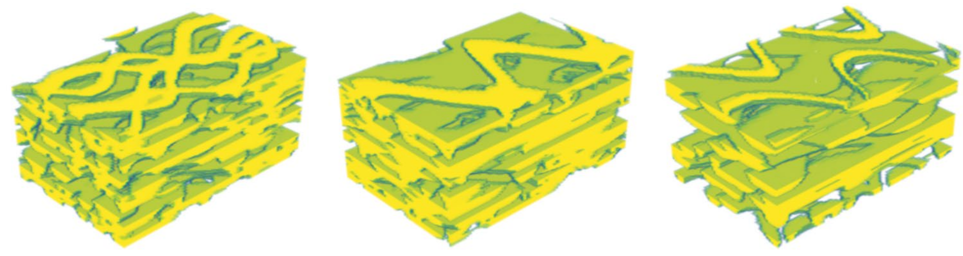


**Fig. 3** Reservoir architecture of the reference scenario and two examples of different geological scenarios. In Example #1, the channel geometries are constrained by facies distributions along the injection and production wells. The facies distribution in the reference scenario is from the reference model in Fig. 1. In Example #2, the channel geometries are not constrained to any data

[37, 39, 40]. In this work, we utilize open-DARTS to perform the simulations [45, 48]. Open-DARTS has been used successfully for ensemble-based simulation of geothermal systems [40]. The simulator employs a fully implicit solution method in time and uses the finite volume method and two-point flux approximation to discretize the standard governing equations for heat and mass transfer in space [49]. The conservation equations are given by

$$\frac{\partial}{\partial t}(\varphi\rho) - \nabla \cdot \rho v + \rho\widetilde{q} = 0 \tag{2}$$

$$\frac{\partial}{\partial t}\left(\varphi\rho U + (1-\phi)U_r\right) - \nabla \cdot h\rho v + \nabla \cdot (\kappa\nabla T) + h\rho\widetilde{q} = 0 \tag{3}$$

where $t$ is the time, $\varphi$ is the porosity of porous media, $\rho$ is the density of fluid phase, $\widetilde{q}$ is the fluid rate per unit volume, $U$ is the phase internal energy, $U_r$ is the internal energy of rock, $h$ is the convection coefficient and $T$ is the temperature. The thermal conductivity of the fluid and rock is defined as

$$\kappa = \varphi\kappa_f + (1-\varphi)\kappa_r \tag{4}$$

where $\kappa$, $\kappa_r$ and $\kappa_f$ are the thermal conduction coefficients of the overall system, the fluid phases and the solid rock, respectively. The Darcy velocity $v$ is given by

$$v = \frac{\mathbf{K}}{\mu}\left(\nabla p - \gamma_p \nabla D\right) \tag{5}$$

where $\boldsymbol{K}$ is the permeability of porous media, $\mu$ is the fluid viscosity, $p$ is the pressure, $\gamma_p$ is the specific weight, and $D$ is the depth. We use pressure and enthalpy as primary variables and consider them as state variables [49], which are evaluated using the Newton–Raphson method when solving for Eqs. (2-3)

$$\frac{\partial g\left(\boldsymbol{\omega}_k\right)}{\partial \boldsymbol{\omega}_k}\left(\boldsymbol{\omega}_{k+1} - \boldsymbol{\omega}_k\right) = -g\left(\boldsymbol{\omega}_k\right) \tag{6}$$

Here, $g$ represents the residual form of the Eqs. (2-3), $\boldsymbol{\omega}$ indicates nonlinear variables represented by pressure and enthalpy in this study, and the subscript $k$ specifies the $k$-th nonlinear iteration. To improve computational efficiency and flexibility of the nonlinear formulation, the operator-based linearization technique is used to compute the Jacobian and residuals [48].

The key simulation parameters are summarized in Table 1. The reservoir is located at a depth of 2,000 m, with dimensions of 3,000 m × 2,000 m × 120 m. The initial reservoir temperature is 353.15 K, and the initial pressure of 200 bar. Porosity and permeability have uniform values of 0.01% and 0.001 mD for the mudstone facies, respectively. The porosity distribution in the sandstone facies is modelled using SGS, as discussed above. The rock thermal conductivity and heat capacity are defined as 3.0 W/m/K and 2,450 kJ/m$^3$/K for the mudstone facies, respectively, and 2.2 W/m/K and 2,300 kJ/m$^3$/K for the sandstone facies. The reservoir is considered to contain water without any dissolved salts or gases, and we assume no interactions, chemically or mechanically, between the geothermal water and the reservoir itself. Cold water is injected at the injection well and hot water is produced from the production well, with an injection and production rate of 10,000 m$^3$/day, and a constant injection temperature of 298.15 K. We simulate 50 years of production. The distance between the injector and producer in the reservoir is 1200 m, with a monitoring borehole located halfway between them (Fig. 1). Horizontal model boundaries are open to flow to mimic an infinitely large reservoir. Vertical model boundaries are closed to flow, and there is no thermal recharge from an overburden or underburden. Note that while these are simplifications, the modelling concept presented here can be readily extended to account for more complex boundary conditions. The model is discretized into 40 m × 40 m × 1 m cells, resulting in a grid size of 75 × 50 × 120 with a total of 450,000 cells.

### 2.3 Ensemble smoother with multiple data assimilation

ES-MDA is applied to the geostatistically generated realizations of the petrophysical property distributions within a given geological scenario, i.e. reservoir architecture. In other words, for a given geological scenario, the channel architecture defined by discrete facies remains fixed, and only the internal property variations within the sandstone facies are updated geostatistically. ES-MDA employs a sequence of inflation factors on the observation error covariance matrix to regulate the update magnitude during each assimilation step. The introduction of inflation factors helps to split the assimilation into multiple smaller updates and prevents overfitting and maintains ensemble variability in the property fields. Key symbols for ES-MDA are summarized in Table 2. The main steps of the ES-MDA algorithm are outlined as follows [26]:

1. Generate 100 prior realizations with heterogeneous properties for a single geological scenario, i.e. reservoir architecture. The ensemble size *Ne* is set to 100 and defined as

**Table 1** Numerical simulation parameters for the geothermal doublet [50]

| Parameters | Values |
|---|---|
| Reservoir dimensions | 3,000 m × 2,000 m × 120 m |
| Injection-production spacing | 1,200 m |
| Well length | 120 m |
| nx, ny, nz | 75, 50, 120 |
| dx, dy, dz | 40 m, 40 m, 1 m |
| Porosity and $k_h$ in sandstone facies | Heterogeneous model: see Fig. 2 and Eq. (1) |
| Porosity and $k_h$ in mudstone facies | 0.0001 and 0.001 mD |
| $k_v/k_h$ | 0.1 |
| Initial reservoir pressure and temperature | 200 bar and 353.15 K |
| Thermal conductivity | 3.0 W/m/K for the sandstone facies, 2.2 W/m/K for the mudstone facies |
| Volumetric heat capacity | 2,450 kJ/m$^3$/K for the sandstone facies, 2,300 kJ/m$^3$/K for the mudstone facies |
| Injection/production rate | 10,000 m$^3$/day |
| Injection temperature | 298.15 K |

**Table 2** Summary of variables used in the ES-MDA framework

| Symbol | Definition | Symbol | Definition |
|---|---|---|---|
| M | ensemble of porosity fields | $\mathbf{d_{obs}}$ | true observations |
| $C_D$ | observation error covariance matrix | $\mathbf{d_{uc}}$ | perturbed observations |
| $C_{DD}$ | covariance matrix of predictions | $i$ | $i$-th ensemble member |
| $C_{YD}$ | cross-covariance matrix between the model prediction and model parameters | $l$ | $l$-th iteration |
| d | observation or prediction vector | $\boldsymbol{\alpha}$ | inflation factor |

$$\mathbf{M} = \left[\mathbf{m}_1, \mathbf{m}_2, \dots, \mathbf{m}_i, \dots \mathbf{m}_{Ne}\right] \tag{7}$$

where $\mathbf{M}$ is the ensemble of porosity fields with an ensemble size of 100. $\mathbf{m}_i$ denotes the porosity field for the $i$-th realization, defined over all grid cells containing sandstone facies, i.e., $\mathbf{m}_i = \left[\varphi_i^1, \varphi_i^2, \dots, \varphi_i^k, \dots, \varphi_i^n\right]$, where $\varphi_i^k$ means the porosity value of the $i$-th realization at the $k$-th sandstone grid cell, and $n$ is the total number of grid cells belonging to the sandstone facies.

2. Define key parameters in ES-MDA. Set the number of iterations $Na$, and the inflation factors $\alpha_l$. $l$ from 1 to $Na$. Here, $\boldsymbol{\alpha} = \left[\alpha_1, \alpha_2, \dots, \alpha_{Na}\right]$ is applied to the measurement error covariance. The inflation factors are used to distribute the data assimilation over multiple iterations instead of assimilating the data in a single step. At each iteration, the observation error covariance $\mathbf{C_D}$ is inflated by $\alpha_l$, resulting in improved stability for nonlinear problems. The observation error covariance for each iteration is given by

$$\mathbf{C}_\mathbf{D}^l = \alpha_l \mathbf{C_D} \tag{8}$$

The inflation factors are required to satisfy $\sum_{l=1}^{Na} 1/\alpha_l = 1$, ensuring that the cumulative effect of the iterative updates is equivalent to a single Bayesian update. Decreasing sequences of $\alpha_l$ are often preferred to allow larger corrections in early iterations and more refined adjustments later. For each ensemble member, perturb the observations using $\mathbf{d}_{uc} = \mathbf{d}_{obs} + \sqrt{\mathbf{C}_\mathbf{D}^l}\mathbf{z_d}$, where $\mathbf{z_d} \sim N\left(0, \mathbf{I}_{Nd}\right)$, and $Nd$ is the total number of measurements assimilated. $\mathbf{d}_{obs}$ identifies the true observation, which is the vector consisting of production temperature, injection pressure, and temperature and pressure profiles along wells at different times. The perturbed observation $\mathbf{d}_{uc}$ ensures that each ensemble member is updated using a statistically consistent method, preserving the correct posterior covariance and preventing ensemble collapse.

3. For all realizations, solve the conservation Eqs. (2) and (3) from time zero until a final time and obtain predictions at the measurement locations (i.e., injector and producer, monitoring borehole, and four virtual lines) across all time steps

$$\mathbf{d}_i^l = G\left(\mathbf{m}_i^l\right) \tag{9}$$

where $\mathbf{m}_i^l$ represents the porosity fields for the $i$-th member at $l$-th iteration. $G(\mathbf{x})$ is a forward model. $\mathbf{d}_i^l$ denotes the prediction vector consisting of measurable quantities such as production temperature and injection pressure, as well as temperature and pressure profiles along the wells.

4. Compute the covariance matrix aswhere $\mathbf{C_{YD}}$ means the cross-covariance matrix between the model prediction and model parameters. $\mathbf{C_{DD}}$ means the covariance matrix of predicted data. For $l = 1$, $\mathbf{m}^l$ and $\mathbf{d}^l$ represent the prior parameters and prior predictions. For $l > 1$, they correspond to posterior parameters and updated predictions from the previous iteration.

 https://doi.org/10.1007/s10596-026-10460-3

$$\mathbf{C_{YD}} = \frac{1}{N_e - 1} \sum_{i=1}^{N_e} \left( \mathbf{m}_i^l - \overline{\mathbf{m}^l} \right) \left( \mathbf{d}_i^l - \overline{\mathbf{d}^l} \right)^T \tag{10}$$

$$\mathbf{C_{DD}} = \frac{1}{N_e - 1} \sum_{i=1}^{N_e} \left( \mathbf{d}_i^l - \overline{\mathbf{d}^l} \right) \left( \mathbf{d}_i^l - \overline{\mathbf{d}^l} \right)^T \tag{11}$$

5. Update the parameter ensemble for the next iteration $l + 1$ using

$$\mathbf{m}_i^{l+1} = \mathbf{m}_i^l + \mathbf{C_{YD}} \left( \mathbf{C_{DD}} + \mathbf{C_D}^l \right)^{-1} \left( \mathbf{d}_{uc,i} - \mathbf{d}_i^l \right), i = 1,2, \ldots, N_e \tag{12}$$

6. Repeat steps 3 to 5 until the maximum number of iterations $Na$ is reached.
7. Posterior ensemble realizations with updated porosity distributions are finally obtained after performing all six previous steps.

### 2.4 Data-worth metrics

Data-worth analysis quantifies the value of data expected from a given observation scheme, typically evaluated by the reduction in the uncertainty in reservoir performance forecast from the prior to the posterior ensemble. Each observation in the calibration dataset is ranked by its effectiveness in reducing the uncertainty of predictions of interest [7]. The prediction uncertainty is defined by

$$Tr(C) = \sum_i \mathrm{Var}\left(d_i\right) \tag{13}$$

where $Tr(*)$ denotes the trace (i.e. sum of diagonal entries) of a matrix. $C$ is the predictive covariance matrix of all observation points, and $d_i$ represents the pressure or temperature at the $i$-th observation in space and time. The trace provides a scalar measure of the total predictive uncertainty across all observations. To quantify the data worth of different measurements, we utilize a commonly considered metric, the trace reduction of the predictive covariance matrix [4, 10, 11] given by

$$\Delta Tr = Tr\left(C_{prior}\right) - Tr\left(C_{post}\right) \tag{14}$$

Here, $C_{\text{prior}}$ is the prior predictive covariance, while $C_{\text{post}}$ represents the posterior predictive covariance after data assimilation. A larger $\Delta Tr$ indicates a higher variance reduction and demonstrates a greater value of data and thus higher data worth, implying a greater contribution of the data acquisition to reducing uncertainty and improving understanding of the geothermal system. Ensemble-based data assimilation enables direct computation of the prior and posterior variances in prediction of reservoir response from the ensemble statistics. Note that the data-worth metrics in this study focus on uncertainty reduction and improvement in model predictions, rather than formal quantities from information theory [51, 52]. The normalized trace reduction is defined to evaluate the relative data worth with respect to the same reference case as

$$Tr_{n,i} = \frac{\Delta Tr_i}{\Delta Tr_{\min}} \tag{15}$$

where, $Tr_{n,i}$ denotes the normalized data worth of $i$-th data acquisition scheme and $\Delta Tr_i$ refers to the absolute data worth. One observation scheme is selected as the reference for data-worth normalization in which only production temperature and injection pressure over the entire production period are observed (see next section). The corresponding data worth is $\Delta Tr_{n,i}$. The larger $Tr_{n,i}$, the greater the uncertainty reduction and value of data for the corresponding data acquisition strategy. Considering the different physical units of pressure and temperature, the prior and posterior predictive covariances are evaluated independently for each variable. The data-worth metrics are normalized and computed separately based on temperature data ($Tr_{Tn}$) and pressure data ($Tr_{Pn}$), respectively. In addition, to evaluate how closely predictions of properties of interest, like temperature and pressure along the well path, match the observation data from the reference case, the root mean square error (RMSE) is used to quantify the deviation from the reference observations. RMSE is defined as

$$RMSE = \sqrt{\frac{1}{N}\sum_{i=1}^{N}\left(S_i - M_i\right)^2} \tag{16}$$

where $S_i$ is the estimated value and $M_i$ is the reference value at any time and position, and $N$ is the total number of ensemble members. A lower RMSE indicates smaller deviation from the reference data and thus better data assimilation performance. Similarly, $\mathrm{RMSE_T}$ and $\mathrm{RMSE_P}$ are calculated separately for temperature and pressure, respectively, based on the corresponding estimated and reference values.

## 2.5 Experimental design

A two-stage investigation of data-worth analysis is conducted. In the first stage, the data worth is analyzed for an equiprobable ensemble of stochastically generated reservoir models that were based on a single geological scenario, i.e. only the reservoir architecture from which the reference model was constructed as shown in Fig. 2. Table 3 summarizes the 16 data-collection cases that are used to evaluate the data worth of different combinations of data types and acquisition strategies, i.e. to quantify which data provide the highest value for reducing uncertainties in production forecast and reservoir response. Among the 16 data-acquisition strategies, Cases #1 to #3 are employed in Sect. 3.2 to evaluate the feasibility of data-worth analysis based on ES-MDA as follows: Case #1: Temperature of the produced fluid ($T_{out}$) and bottom hole pressure at the injection well ($P_{inj}$), which

**Table 3** Case design for different data acquisition schemes

| Case | Observation type(s) | Observation location(s) | Period | Note |
|---|---|---|---|---|
| #1 | $T_{out}$ and $P_{inj}$ | INJ & PRD wellhead | 50 yr | / |
| #2 | Well $T$ and $P$ profiles | INJ, PRD, MON | 50 yr | / |
| #3 | $T_{out}$, $P_{inj}$, Well $T$ and $P$ profiles | INJ & PRD well head; distributed T & P along PRD | 50 yr | / |
| #4 | Well $T$ profiles | INJ, PRD, MON | 50 yr | Data type |
| #5 | Well $P$ profiles | INJ, PRD, MON | 50 yr | |
| #6 | Well $T$ and $P$ profiles | INJ | 50 yr | Number and locations of monitoring boreholes |
| #7 | Well $T$ and $P$ profiles | PRD | 50 yr | |
| #8 | Well $T$ and $P$ profiles | MON | 50 yr | |
| #9 | Well $T$ and $P$ profiles | INJ, PRD | 50 yr | |
| #10 | Well $T$ and $P$ profiles | INJ, PRD, three vertical monitoring boreholes evenly spaced along the INJ-PRD line | 50 yr | |
| #11 | Well $T$ and $P$ profiles | INJ, PRD, three vertical monitoring boreholes evenly spaced along a line perpendicular to the INJ-PRD line | 50 yr | |
| #12 | Well $T$ and $P$ profiles | INJ, PRD, Deviated MON | 50 yr | Configuration of monitoring boreholes |
| #13 | Well $T$ and $P$ profiles | INJ, PRD, Horizontal MON (2000 m) | 50 yr | |
| #14 | Well $T$ and $P$ profiles | INJ, PRD, Horizontal MON (2060 m) | 50 yr | |
| #15 | $T_{out}$ and $P_{inj}$ | INJ & PRD wellhead | Varied[1] | Observation period |
| #16 | Well $T$ and $P$ profiles | INJ, PRD, MON | Varied[1] | |

[1]Varied observation intervals: 0 to 1, 0 to 3, 0 to 5, 0 to 10, 0 to 15, 0 to 20, 0 to 25, 0 to 30, 0 to 40, and 0 to 50 years

https://doi.org/10.1007/s10596-026-10460-3

are the easiest data to obtain from the field. Case #2: Temperature and pressure profiles along the injection well (INJ), monitoring borehole (MON), and production well (PRD), collected using Optical Fiber sensors distributed along the wells. Case #3: The $T_{out}$, $P_{inj}$, and temperature and pressure profiles along the PRD. Cases #4 to 16 are employed in Sect. 3.3 to investigate the effects of types of observed variables (Cases #4 and #5), number and locations of monitoring boreholes (Cases #6 to #11), configurations of monitoring boreholes (Cases #12 to #14), and periods of the observations (Case #15 and #16) on data worth. In Case #10, three monitoring boreholes are evenly distributed along the injector-producer line; in Case #11, three monitoring boreholes are arranged perpendicular to the injector-producer line. Case #2 consider a vertical monitoring borehole, Case #12 a deviated monitoring borehole, and Cases #13 and #14 horizontal monitoring boreholes located at the top of the reservoir (depth 2000 m) and at mid-reservoir depth (2060 m), respectively, as shown in Fig. 4. We note that some of these cases would not be considered in real geothermal operations because it would be prohibitively expensive to drill additional monitoring boreholes. However, these cases allow us to quantify how additional data helps in constraining uncertainties in the production forecasts.

In the second stage, we examine how the data-worth analysis changes if the ensemble is based on a geological scenario that differs from the reservoir architecture that is present in the subsurface. To this end, ten additional geological scenarios are considered. Among these, five geological scenarios honor the facies recorded along injection and production wells from the reference model, and Example#1 is one of these constrained scenarios (Fig. 3). In addition, five scenarios are generated without any facies constraints, and Example #2 represents one of these unconstrained scenarios (Fig. 3). Comparing these scenarios allows us to investigate how sensitive the data-worth analysis is to uncertainty in the conceptual geological model space. These results are presented in Sect. 3.4.

# 3 Results

## 3.1 Uncertainty analysis

In this section, the resulting uncertainties in the reservoir performance forecasts due to the variability in reservoir properties are quantified, while we are using a single, fixed geological scenario as shown in Fig. 2. Uncertainty in the production forecasts, for example the temperature of the produced fluid ($T_{out}$) and the bottom hole pressure at the injection well ($P_{inj}$), is presented. Uncertainty in temperature and pressure profiles along the injector and

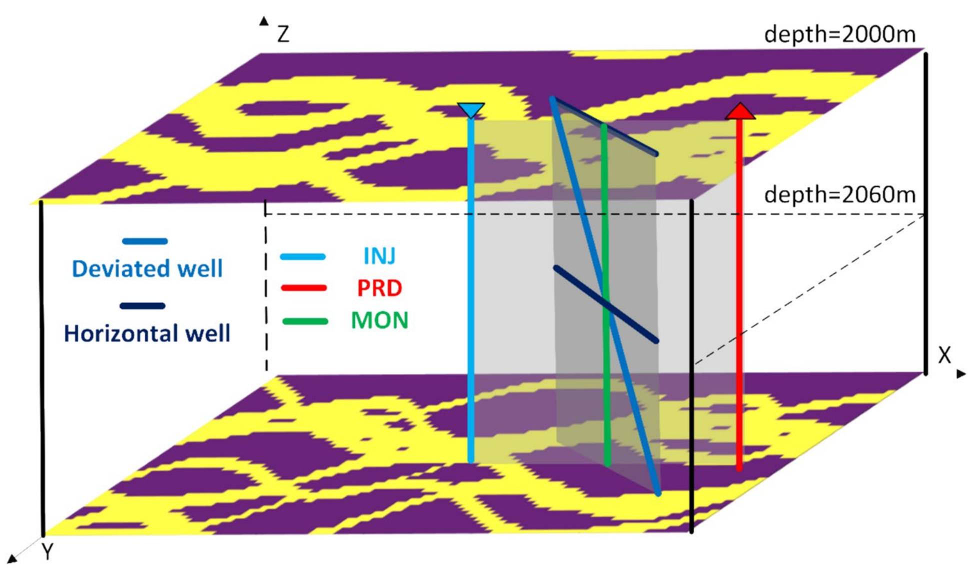


**Fig. 4** 3D configurations of monitoring boreholes, i.e. virtual lines along which data is recorded. Blue, green, and red lines represent the injector, vertical monitoring borehole, and producer, respectively; dark blue lines indicate horizontal monitoring boreholes at different depths; the slanted blue line denotes a deviated monitoring borehole. Deviated and horizontal monitoring boreholes are positioned in a plane intersecting the injection–production plane (dark shading), enabling coverage of a larger reservoir region

producer wells as well as the monitoring borehole is analyzed to determine the depths and time intervals that exhibit the largest variability in the temperature and pressure profiles.

#### 3.1.1 Uncertainty in the production forecasts

Thermal breakthrough occurs after approximately 20 years, as shown in the evolution of $T_{out}$ and $P_{inj}$ for the 100 equiprobable realizations (Fig. 5). The uncertainty interval is indicated by the P10 to P90 interval. The P10 to P90 interval of the $T_{out}$ gradually widens, indicating increasing uncertainty over time as the cold front propagates from the injection well towards the producer, and the variability in the flow paths increases, which is related to the geological variability captured in the reservoir model ensemble. Injection pressure increases steadily as the cooling of the reservoir increases the fluid viscosity and hence flow resistance. The P10 to P90 interval of $P_{inj}$ remains relatively stable over time because pressure diffusion occurs on much shorter time scales compared to heat flow, causing a quasi-steady-state pressure field to be established quickly. After 50 years of production, the maximum P10 to P90 interval is approximately 1.9 K for the temperature of the produced fluid and 2.0 bar for injection pressure. When assuming a 5 K decline in $T_{out}$ as the abandonment criterion, the P10 to P90 interval defining the uncertainty in the lifespan of the geothermal system varies between 37 and 43 years.

#### 3.1.2 Uncertainty in temperature and pressure profiles

The simulated temperature and pressure profiles along the injection well, monitoring borehole, and production well vary with time and space as presented in Fig. 6. The temperature profiles show inflection points along the wellbore, reflecting the impact of different reservoir layers on flow rates. Local low-temperature segments correspond to depths where strong convective heat transport occurs, indicating a faster advance of the cold front and the presence of connected sandstone facies with higher permeability. Conversely, higher-temperature segments suggest less convective transport, indicating either disconnected sandstone facies or low-permeability mudstone facies. These regions exchange heat with each other due to thermal conduction, resulting in gradual variations of temperature between the low- and high-permeability facies. The maximum P10 to P90 interval varies between wells, with 14.5 K for the injection well at year 1, 15.2 K for the monitoring borehole at year 30, and 8.9 K for the production well at year 50. The pressure profiles along the wells show more abrupt changes and inflections as a function of depth. These abrupt changes are because pressure is sensitive to permeability variations and channel geometry and connectivity. Along the wells, regions where pressure remains close to the initial reservoir pressure indicate low-permeability mudstone facies, while regions where pressure drops below the initial pressure indicate connected sandstone facies. The maximum P10 to P90 interval varies between wells, with 1.24 bar for the injection well at year 1, 0.48 bar for the monitoring borehole at year 30, and 1.20 bar for the production well at year 50.

The uncertainty in temperature profiles recorded along the three wells evolves as a function of time and depth (Fig. 7). In the first five years, the temperature profile along the injection well exhibits higher uncertainty as cold water starts to move into the formation. From year 10 to year 50, larger uncertainties are observed at the

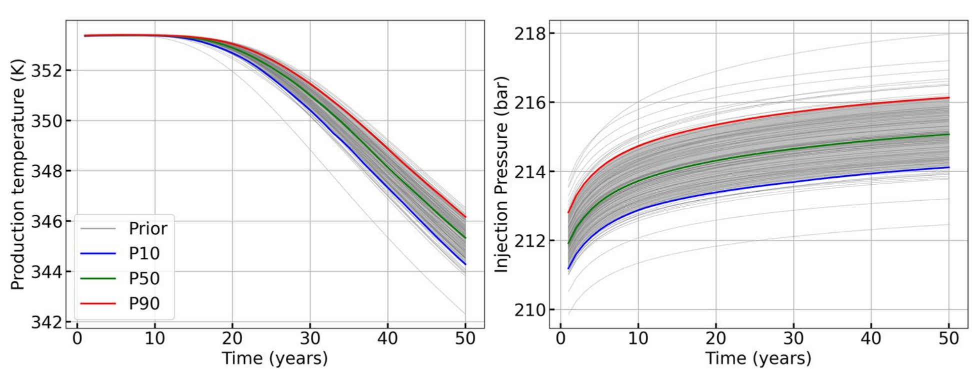


**Fig. 5** Simulated evolution of the temperature of the produced fluid ($T_{out}$) and bottom hole pressure at the injection well ($P_{inj}$) for 100 equiprobable realizations. Grey lines represent individual realizations. The shaded grey area between the P10 and P90 indicates the uncertainty interval

 https://doi.org/10.1007/s10596-026-10460-3

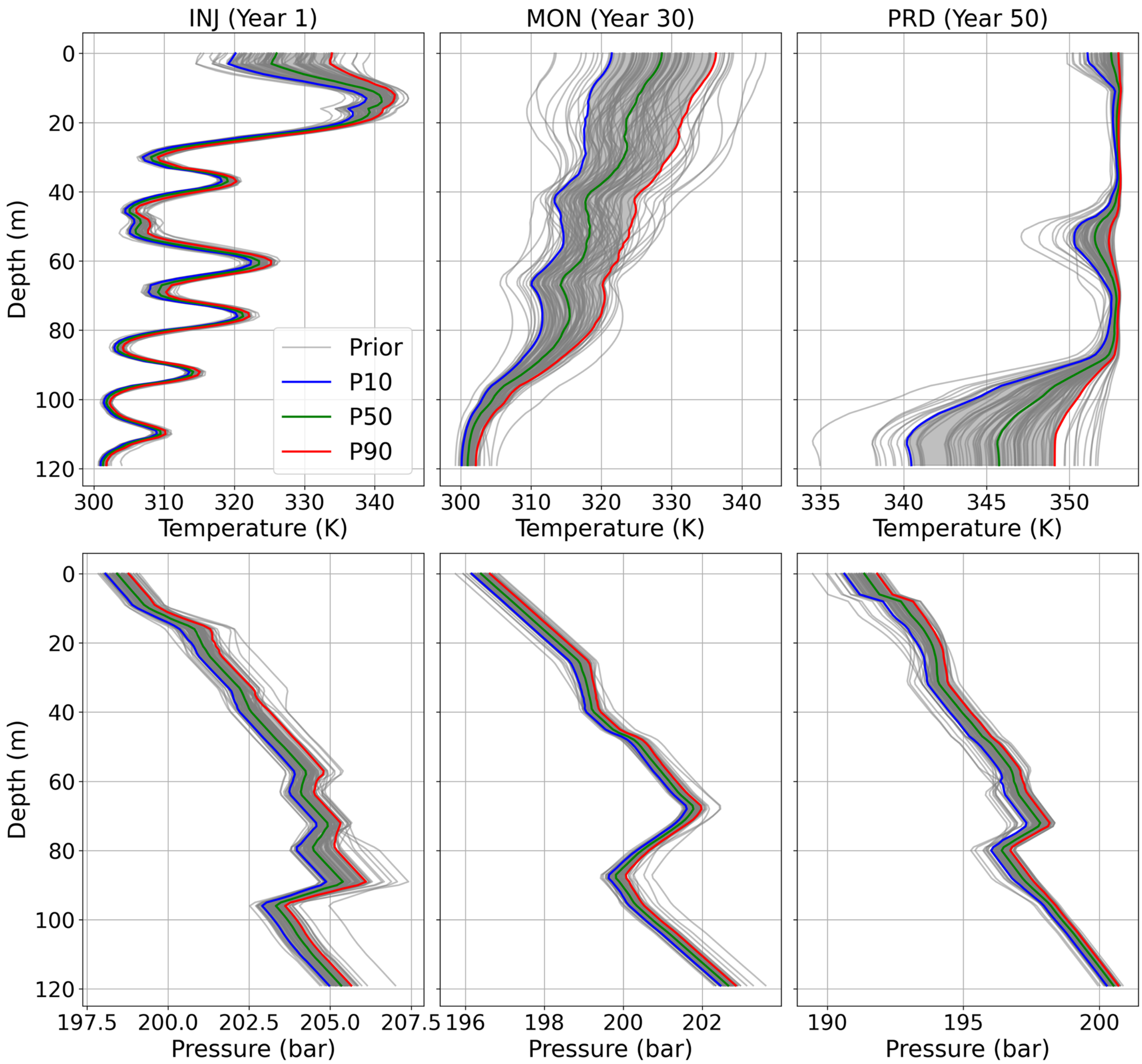


**Fig. 6** Temperature and pressure profiles as a function of depth for the injector, monitoring borehole, and producer, after 1, 30 and 50 years of production, respectively (from left to right). Thin grey lines show the predictions for 100 equiprobable realizations of the reference scenario

monitoring borehole, indicating that this data provides valuable information because it captures the arrival and passage of the cold front. At the production well, an increase in uncertainty only starts to occur after 40 years once the cold front arrives, with limited information before then. The uncertainty in temperature also varies with depth. For the injection well and the monitoring borehole, a larger uncertainty is observed in the upper layers, suggesting the presence of locally connected high-permeability channels that facilitate heat convection and conductive heat exchange between the low- and high-permeability facies. In contrast, at the production well, uncertainty is more pronounced at the bottom of the reservoir, implying the existence of locally connected high-permeability channels and faster heat convection. Overall, uncertainty in the temperature profile is greater at the monitoring borehole than at the injection well, followed by the production well. As discussed above, the variability in temperature uncertainty is caused by the propagation of the cold front.

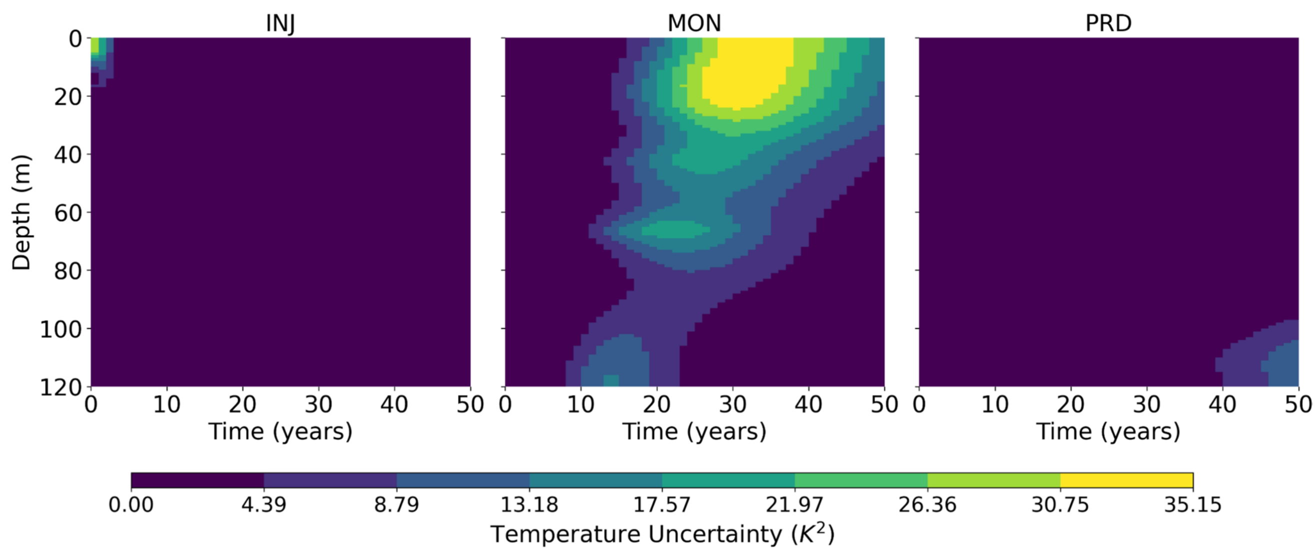


**Fig. 7** Uncertainty maps for the temperature profiles recorded along the injector (INJ), monitoring borehole (MON), and producer (PRD) as functions of time and depth. Colors indicate the degree of uncertainty, calculated from the variance of ensemble members at each time and depth (Eq. 12). Dark colors refer to lower uncertainty bright colors to larger uncertainty

Similar to the temperature profiles, the uncertainty in the pressure profiles recorded along the three wells also evolves as a function of time and depth (Fig. 8). During the production, the uncertainty in pressure profiles increase slightly with time along the injection and production wells, whereas it remains near zero at the monitoring borehole. The slight increase in uncertainty is due to the gradual temperature decrease in the reservoir, which increases fluid viscosity and flow impedance. Overall, uncertainty in the pressure profile is greater at the injection well than at the production well, followed by the monitoring borehole. The result is consistent with the source–sink dynamics of the flow process. The uncertainty in pressure also varies with depth. For the injection

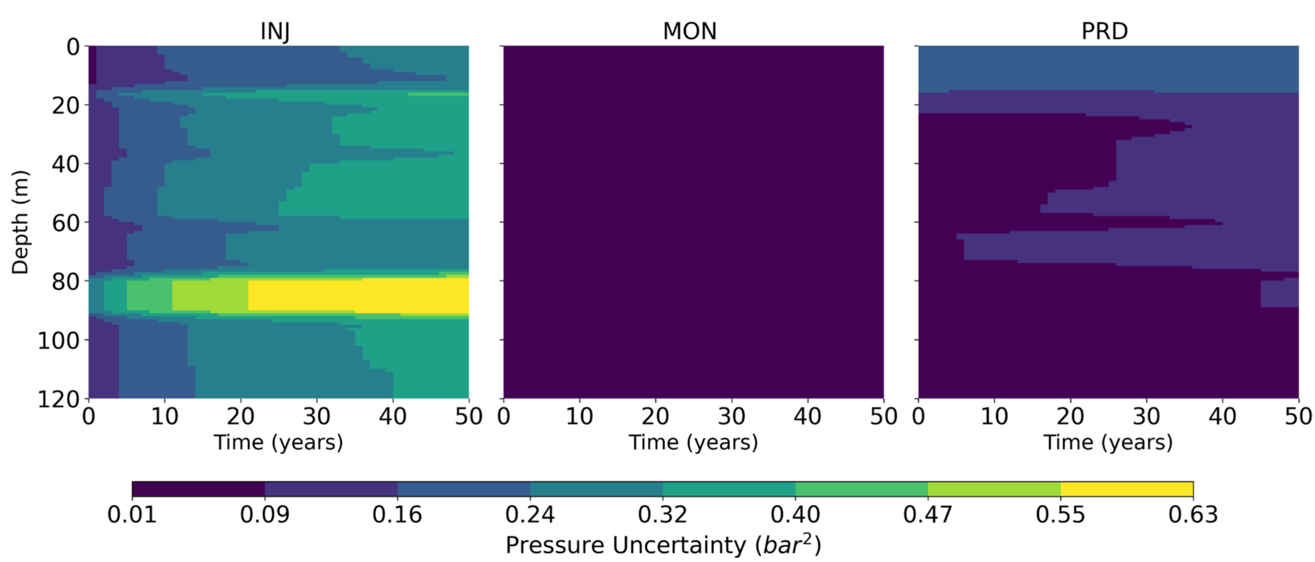


**Fig. 8** Uncertainty maps for the pressure profiles recorded along the injector (INJ), monitoring borehole (MON), and producer (PRD) as functions of time and depth. Colors indicate pressure uncertainty, calculated from the variance of ensemble members at each time and depth (Eq. 12). Dark colors refer to lower uncertainty bright colors to larger uncertainty

 https://doi.org/10.1007/s10596-026-10460-3

well, the largest uncertainty occurs between depths of 80 to 90 m, suggesting the presence of connected sandstone layers. For the production well, the increased uncertainty at depths of 0 to 16 m indicate a more connected layer. However, these layers do not necessarily indicate preferential flow pathways since heat transfer is slower than fluid flow and also affected by thermal conduction.

Although the changes in the temperature profiles are more gradual compared to the pressure profiles, the inflection points in both profiles can be used to assess the reservoir connectivity and the structure of the reservoir layers. The uncertainty in the temperature profiles is significantly higher than the uncertainty in the pressure profiles, including a larger P10 to P90 interval. This is because pressure equilibrates more rapidly, whereas temperature is governed by the slower propagation of the cold front and the conductive heat exchange between low- and high-permeability regions. Pressure profiles, however, show more variation along the wells compared to temperature profiles. Unlike temperature, which is mainly informative during thermal breakthrough, pressure profiles retain value of data at all stages, even in the absence of a discernible cold front. In the following section, temperature and pressure profiles from the three wells are incorporated as observations in the data assimilation process to constrain uncertainties in production performance and reservoir response.

## 3.2 Data-worth analysis based on ES-MDA

We now conduct data assimilation using different combinations of the data recorded at the three wells, again focusing on the reference geological scenario. During ES-MDA, only the permeability and porosity within the channelized sandstone facies are updated, the reservoir architecture remains fixed for a given geological scenario [42]. Based on the simulated results of the prior and posterior ensembles, data worth values are calculated to assess the contribution of the different data types and amounts.

ES-MDA parameters are summarized in Table 4. The observation data consists of the temporal evolution of the temperature and pressure profiles recorded along the injector, monitoring borehole, and producer for the reference case, as well as $T_{out}$ and $P_{inj}$ at the injector for the reference case. Observation errors are set to 1 K for temperature and 2 bar for pressure, based on typical monitoring equipment. Four iterations are performed with inflation factors (Eq. (12)).

### 3.2.1 Data assimilation for case #1

Case #1 uses the temperature of the produced fluid ($T_{out}$) and the bottom hole pressure at the injection well ($P_{inj}$) as observations. The prior predictions, posterior predictions, and reference data for the $T_{out}$ and $P_{inj}$ are compared in Fig. 9. After data assimilation, using the full 50 years of observations, the posterior ensemble aligns more closely with the observation data from the reference case. The maximum P10 to P90 interval decreases from 1.9 K to 0.6 K for $T_{out}$ and from 2.0 bar to 1.7 bar for $P_{inj}$ respectively. The reduction in uncertainty is more pronounced for $T_{out}$ than for $P_{inj}$.

**Table 4** ES-MDA parameters

| Parameters | Values |
|---|---|
| Number of iterations | 4 |
| Ensemble size | 100 |
| Inflation factor | [9.43, 7, 4, 2] |
| Observations | Production data or temporal evolution of temperature and pressure profiles along wells simulated in the reference case |
| Observation error | 1 K for temperature and 2 bar for pressure |
| Lower and upper limits of porosity | 0.125 to 0.32 |

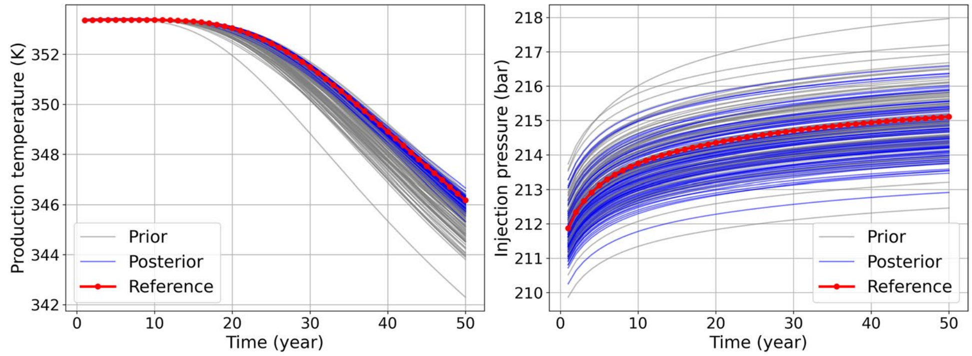


**Fig. 9** Simulated $T_{out}$ and $P_{inj}$ for the prior and posterior ensembles of the reservoir architecture for the reference case, using the observation data for Case #1. The red line represents the production response from the reference case. The grey lines are predictions from the prior ensemble; the blue lines are results from the posterior ensemble

When comparing the temperature and pressure profiles for the prior and posterior ensembles at the injecton well, monitoring borehole, and production well, and the four virtual lines, the P10 to P90 intervals are only slightly reduced (Fig. 10). This indicates that the uncertainty in the reservoir forecasts remains high and that it is difficult to quantify the reservoir dynamics. Data worth values calculated from the four virtual lines yield a $Tr_T$ of 4523.69 $K^2$ and $Tr_p$ of 23.09 $bar^2$. In summary, the observation data in Case #1 helps to constrain the uncertainty in the production forecasts but provides little information that helps to constrain the uncertainty in reservoir temperature and pressure. This result highlights a common problem with data assimilation and history matching: because the problems are ill-posed, it is possible to obtain 'the right answer for the wrong reason', i.e. be able to match the production behaviour without matching the actual dynamics and flow behaviour in the reservoir which undermines the reliability of the production forecasts.

### 3.2.2 Data assimilation for case #2

Case #2 uses the temperature and pressure profiles along INJ, MON, and PRD as observations. The prior predictions, posterior predictions, and reference data for $T_{out}$, $P_{inj}$, and the temperature and pressure profiles

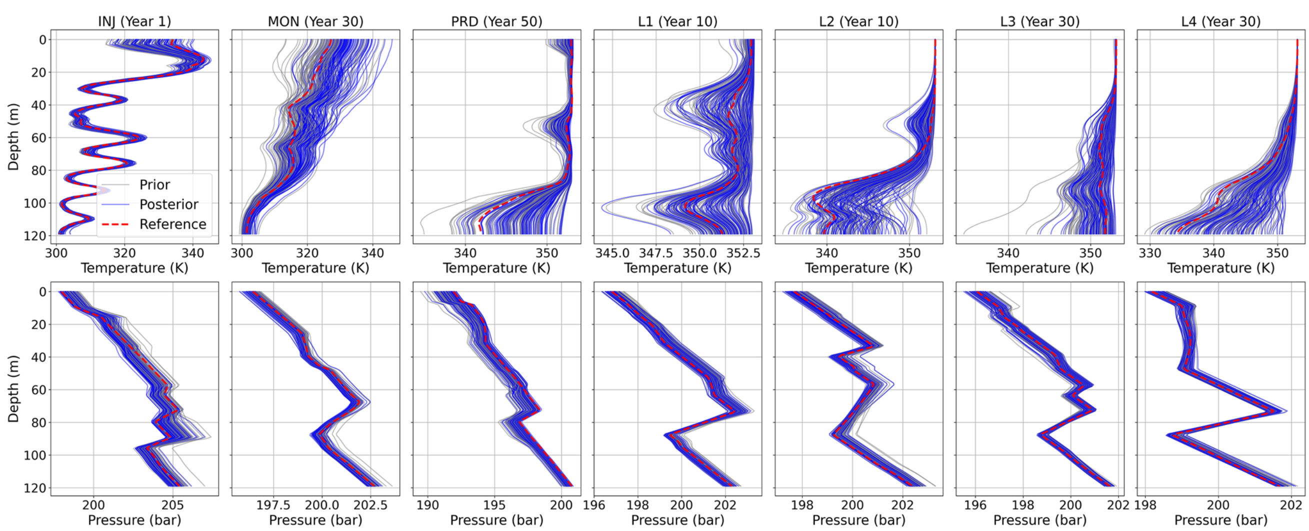


**Fig. 10** Prior, posterior, and reference temperature and pressure profiles recorded as a function of depth for the injection well (INJ), monitoring borehole (MON), production well (PRD) and four virtual lines (L1 to L4) at different times, respectively (from left to right) for the observation data from Case #1. The grey lines show the forecasts for the prior ensemble, the red line denotes the reference data for the reference case, and the blue lines are the predictions for the posterior ensemble after data assimilation

 https://doi.org/10.1007/s10596-026-10460-3

in Case #2 are compared in Figs. 11 and 12. After data assimilation, the posterior temperature and pressure profiles along the injection well, production well, and monitoring borehole show substantial reduction of the P10 to P90 intervals and match the reference curves more closely. Posterior $T_{out}$ and $P_{inj}$ also align more closely with the reference data from the reference case and exhibit a reduced maximum P10 to P90 interval (from 1.9 K to 0.7 K, and from 2.0 bar to 0.6 bar), even though $T_{out}$ and $P_{inj}$ were not assimilated in Case #2. At the four virtual lines, posterior profiles display a reduced uncertainty compared to Case #1. The data worth values in Case #2, $Tr_T = 17169.82$ K$^2$ and $Tr_P = 66.82$ bar$^2$, are higher than those in Case #1, indicating that the uncertainty in the reservoir forecasts is lower and the reservoir dynamics are better constrained. In summary, the observation data in Case #2 provides more effective information to help constrain the uncertainty in both, production forecasts and reservoir temperature and pressure.

### 3.2.3 Normalized data-worth analysis

The normalized data worth is calculated to highlight the relative value of data for each acquisition strategy and enable an objective comparison across the different strategies. The data worth is normalized to that of

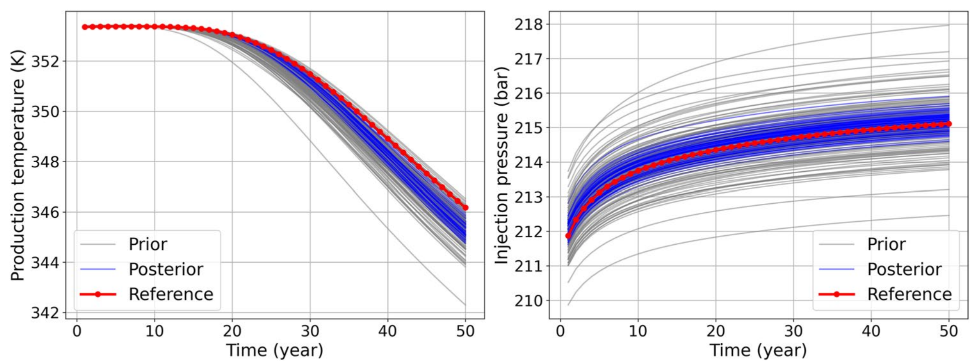


**Fig. 11** Simulated $T_{out}$ and $P_{inj}$ for the prior and posterior ensembles of the reference scenario using the observation data of Case #2. See Fig. 9 for the definitions of the colored lines

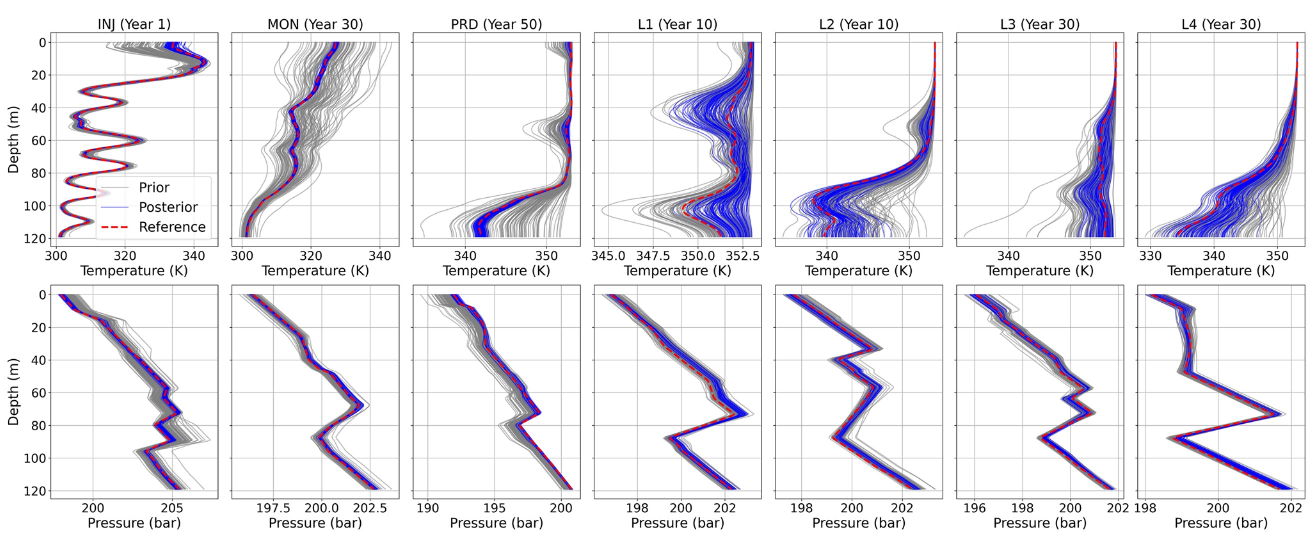


**Fig. 12** Prior, posterior, and reference temperature and pressure profiles recorded as a function of depth for the injection well (INJ), monitoring borehole (MON), production well (PRD) and four virtual lines (L1 to L4) at different times, respectively (from left to right) for the observation data from Case #2. See Fig. 10 for the definitions of the colored lines

Case #1 (Eq. (15)). Case #3 uses $T_{out}$, $P_{inj}$, and the temperature and pressure profiles along the PRD for data assimilation. The histogram of the normalized data-worth results for Cases #1 to #3 are presented in Fig. 13 where $Tr_{T_n}$ and $Tr_{P_n}$ are normalized data worth based on temperature and pressure profiles, respectively, along the four virtual lines. In Case #3, $T_{out}$ and $P_{inj}$ are assimilated together with temperature and pressure profiles along the single production well. Case #3 yields approximately twice the data worth value of Case #1, indicating that adding temperature and pressure profiles along the production well can further reduce uncertainty in the production forecasts and better constrain the reservoir dynamics compared to a data acquisition scheme that only uses $T_{out}$ and $P_{inj}$. Case #2 achieves more than three times the normalized data worth than Case #1. This result suggests that data acquisition schemes that monitor the temperature and pressure profiles along several wells, e.g. using fiber optics installed in the wells, result in substantially higher data worth compared to acquisition schemes that only monitor $T_{out}$ and $P_{inj,}$ e.g. measured by thermocouple and permanent downhole pressure gauge respectively.

## 3.3 Impact of different types of observation on data worth

To investigate the impact of different types of observation on data worth, we conduct data assimilation using the observations from 13 more cases (#4 to #16) as shown in Table 3. As discussed previously, these observations vary in the types of observation data (temperature or pressure), the number and locations of monitoring boreholes, the configuration of monitoring boreholes (deviated, shallow horizontal or deep horizontal borehole), and the observation period. This section aims to give insight into the value of different data acquisition strategies. Case #2 is selected as the reference strategy for comparison because it covers relatively complete observations from injector, producer, and monitoring borehole. Note that all data worth values are normalized with respect to Case#1.

### 3.3.1 Types of observed variables

Cases #4 and #5 use either the temperature or the pressure profiles along the injector, monitoring borehole, and production well. Temperature profiles yield about 50% higher data worth than pressure profiles (Fig. 14), indicating that 50-year temperature observations provide greater information for constraining reservoir dynamics. The result is consistent with the previous uncertainty analysis, where pressure profiles display a narrower P10 to P90 interval than temperature profiles, reflecting their lower information. The underlying reason is that fluids

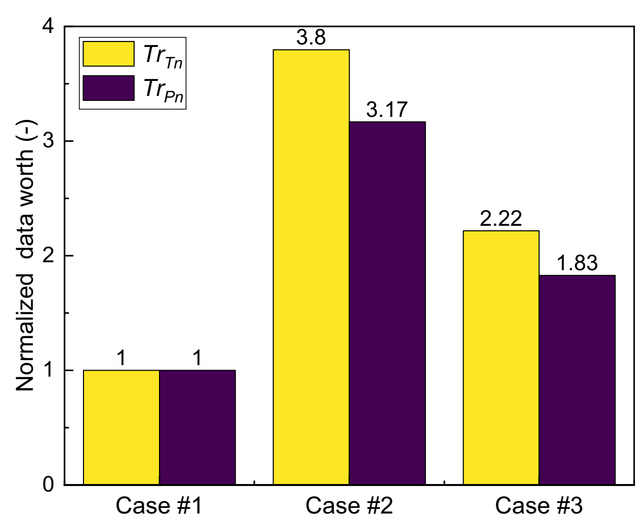


**Fig. 13** Histogram of normalized data worth for Cases #1, #2, and #3. All data-worth values are normalized with respect to Case #1. Yellow and purple bars represent data worth based on temperature and pressure profiles, respectively, along four virtual lines

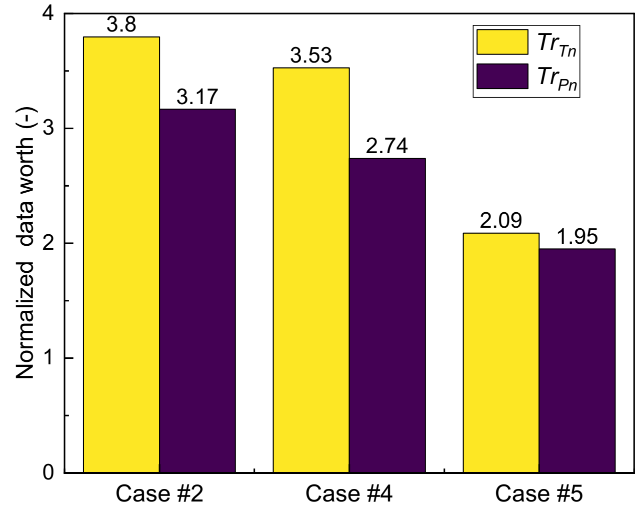


**Fig. 14** Histogram of normalized data worth for Cases #2, #4, and #5, showing the effect of observation data types. All data worth values are normalized with respect to Case #1. The colors of the individual bars are the same as in Fig. 13

are injected and produced at a constant rate and hence the pressure field equilibrates rapidly. Pressure therefore remains relatively constant and only response to the increase in the viscosity as the reservoir cools during the propagation of the cold front.

The data-worth analysis of Case #2 uses the pressure and temperature profiles, i.e. is a combination of the individual datasets based on which the data-worth analyses for Cases 4 and #5 are performed. However, the data worth of Case #2 is not the sum of the data worths of Cases #4 and #5. From Case #2 to Case #4, additional pressure profiles are recorded, but there is only a small increase in data worth, 0.27 in $Tr_{Tn}$ and 0.43 in $Tr_{Pn}$, which indicates redundancy in the data types. As discussed above, the evolution of the temperature and pressure profiles are both a result of the connectivity of the fluvial channels and the permeability contrast between the sand and mudstone facies. That is, temperature and pressure profiles are not independent datasets and hence data type redundancy arises.

#### 3.3.2 Number and locations of monitoring boreholes

The histogram of normalized data worth for Cases #2 and #6 to #11 illustrates the influence of both, the number and locations of the monitoring boreholes (Fig. 15). Cases #6, #7, and #8 are based on the temperature and

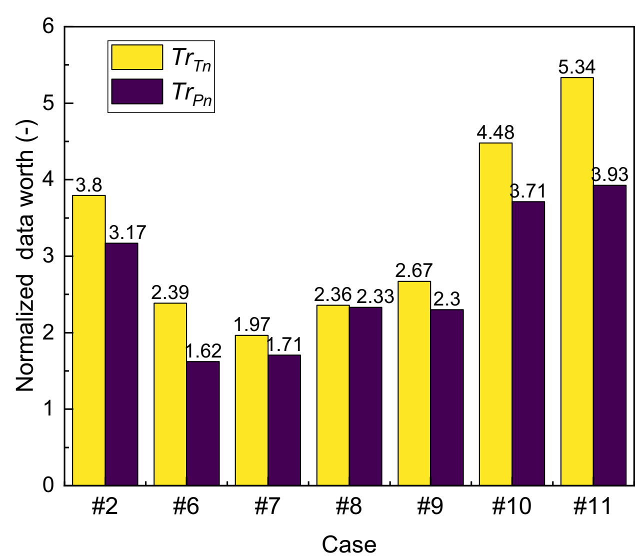


**Fig. 15** Histogram of normalized data worth for Cases #2, #6 to #11, showing the effect of the number and locations of monitoring boreholes. All data worth values are normalized with respect to Case #1. The colors of the individual bars are the same as in Fig. 13

pressure profiles recorded along either the injection well, the production well, or the monitoring borehole, respectively. The monitoring borehole provides the greatest reduction in uncertainty for both, reservoir temperature and pressure, as it captures more of the propagation of the cold front compared to the injection or production wells. The data worth increases if the number of wells along which temperature and pressure profiles are recorded increases from 2, 3, and 5 wells (Cases #9, #2, and #10). Case #9 uses the injector and producer (two wells), Case #2 adds one monitoring borehole (three wells), and Case #10 considers three monitoring boreholes in addition to the injector and producer. We reiterate that some of these configurations will not be applicable in real geothermal systems but still allow us to quantify how the value of data for different observation strategies changes. The three monitoring boreholes are equally spaced along a virtual line that connects the injector and producer. Case #11 also considers three monitoring boreholes, but they are placed perpendicular to this line. The data acquisition strategy in Case #11 yields higher data worth compared to Case #10, as it captures more of the cross-sectional flow between the injector and producer rather than only the main injection–production axis.

#### 3.3.3 Configurations of monitoring boreholes

The histogram of normalized data worth for different orientations of the monitoring borehole (Fig. 16) reveals that both, a deviated and a horizontal monitoring borehole, yield higher data worth compared to a vertical borehole because they capture flow and heat-transfer information in a direction other than main flow direction line, i.e. sample more of the propagation of the cold front. As noted above, the direct-use geothermal systems will rarely have monitoring boreholes so if they do, this analysis helps quantify the change in value of data for different well orientations. The data worth of the deviated borehole is comparable to that of the horizontal borehole. The data worth of a horizontal monitoring borehole also depends on the depth at which it is located. The results highlight that the configurations of borehole can have impact on the value of monitoring data.

#### 3.3.4 Periods of observation

To evaluate the impact of dynamic observations on data worth, Cases #15 and #16 were designed to assimilate observations collected over different time intervals, i.e. 1, 3, 5, 10, 15, 20, 25, 30, 40, and 50 years from the start of production. Case #15 assimilates observations of $T_{out}$ and $P_{inj}$ over these intervals, whereas Case #16 assimilates temperature and pressure profiles recorded along the injector, producer, and monitoring borehole. For Case #15, the data worth remains almost unchanged and even decreases when the time interval for the observations is less than 20 years (Fig. 17). Once the time interval for the observations exceeds 20 years, data worth increases, indicating that the uncertainty in reservoir temperature and pressure starts to decrease after

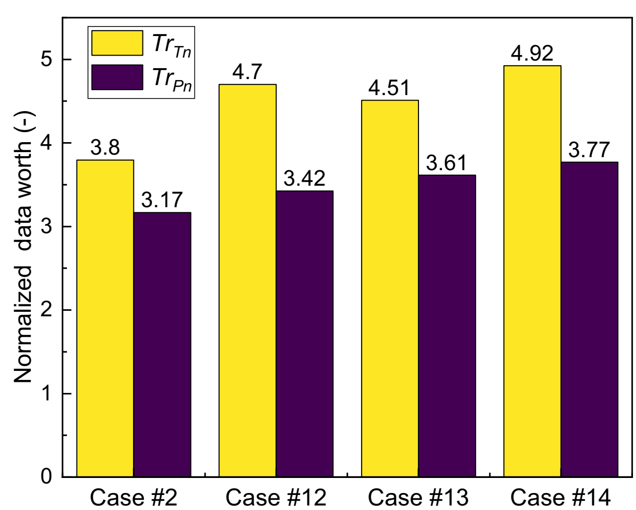


**Fig. 16** Histogram of normalized data worth for Cases #2, #12 to #14, showing the effect of configurations of monitoring boreholes. The colors of the individual bars are the same as in Fig. 13

**Fig. 17** Histograms of normalized data worth for Case #15 and #16, showing the effects of the periods of observations for well temperature and pressure profiles along the injector (INJ), producer (PRD), and monitoring (MON) wells and boreholes (upper figure) and the effects of the periods of observations for $T_{out}$ and $P_{inj}$ (lower figure), respectively. All data worth values are normalized with respect to Case #1. The colors of the individual bars are the same as in Fig. 13

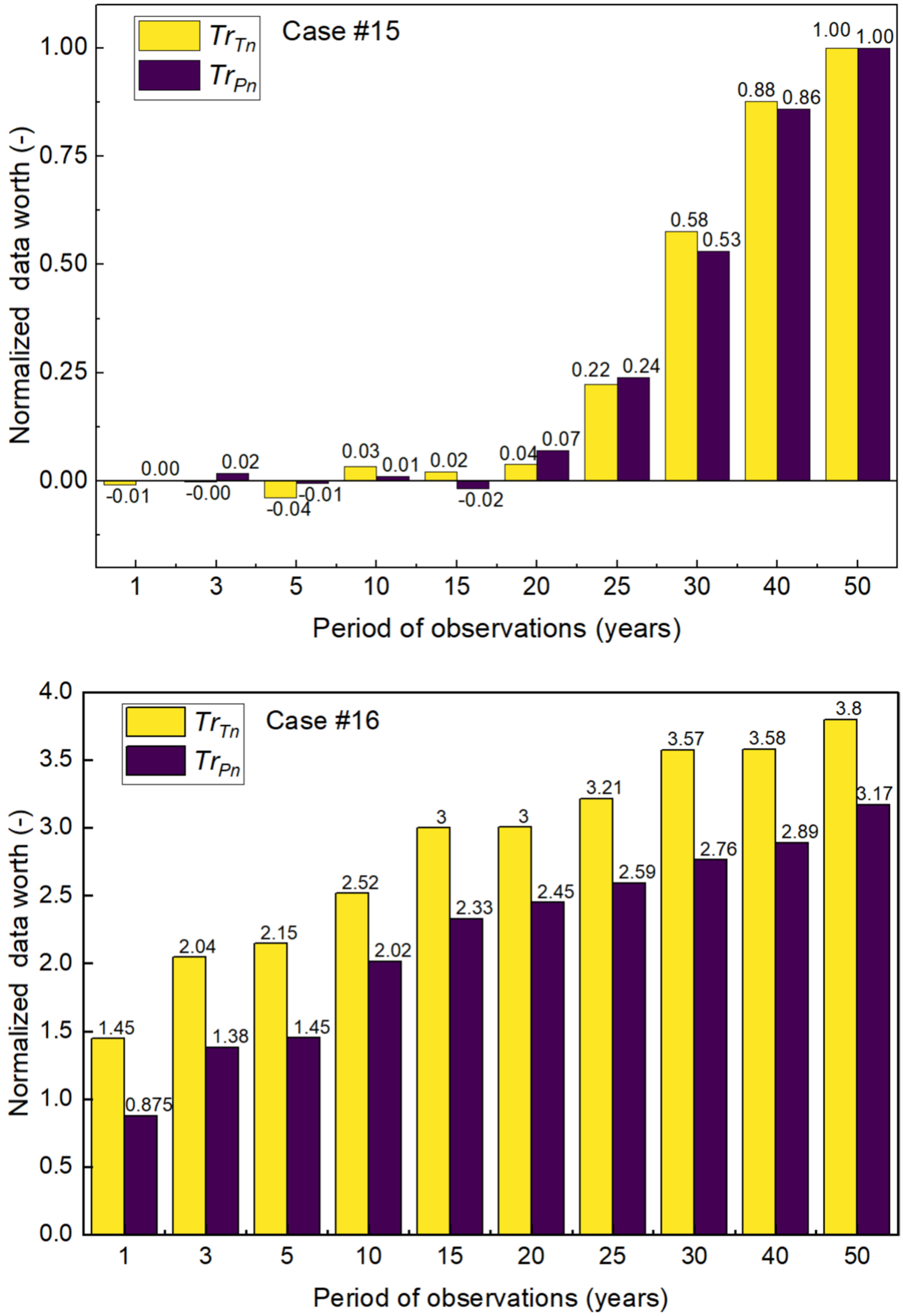


approximately 20 years of observation for $T_{out}$ and $P_{inj}$. The P10 to P90 interval for $T_{out}$ and $P_{inj}$ for the entire 50 years of production are also presented to illustrate how uncertainty in production performance varies as a function of the observation period (Fig. 18). Assimilating a time interval of less than 20 years for the observations of $T_{out}$ and $P_{inj}$ results in nearly constant P10 to P90 intervals (1.9 K, 2.0 bar, and 5.3 years) which are identical to the prior P10 to P90 intervals. In contrast, considering a time interval of more than 20 years for the observations leads to a gradual decrease of the P10 to P90 interval, with values of 1.35 K, 1.77 bar, and 4.00 years when observations from a 30-year time interval are assimilated, and 0.64 K, 1.73 bar, and 1.76 years when the full 50 years of production data are assimilated. As discussed above, thermal breakthrough

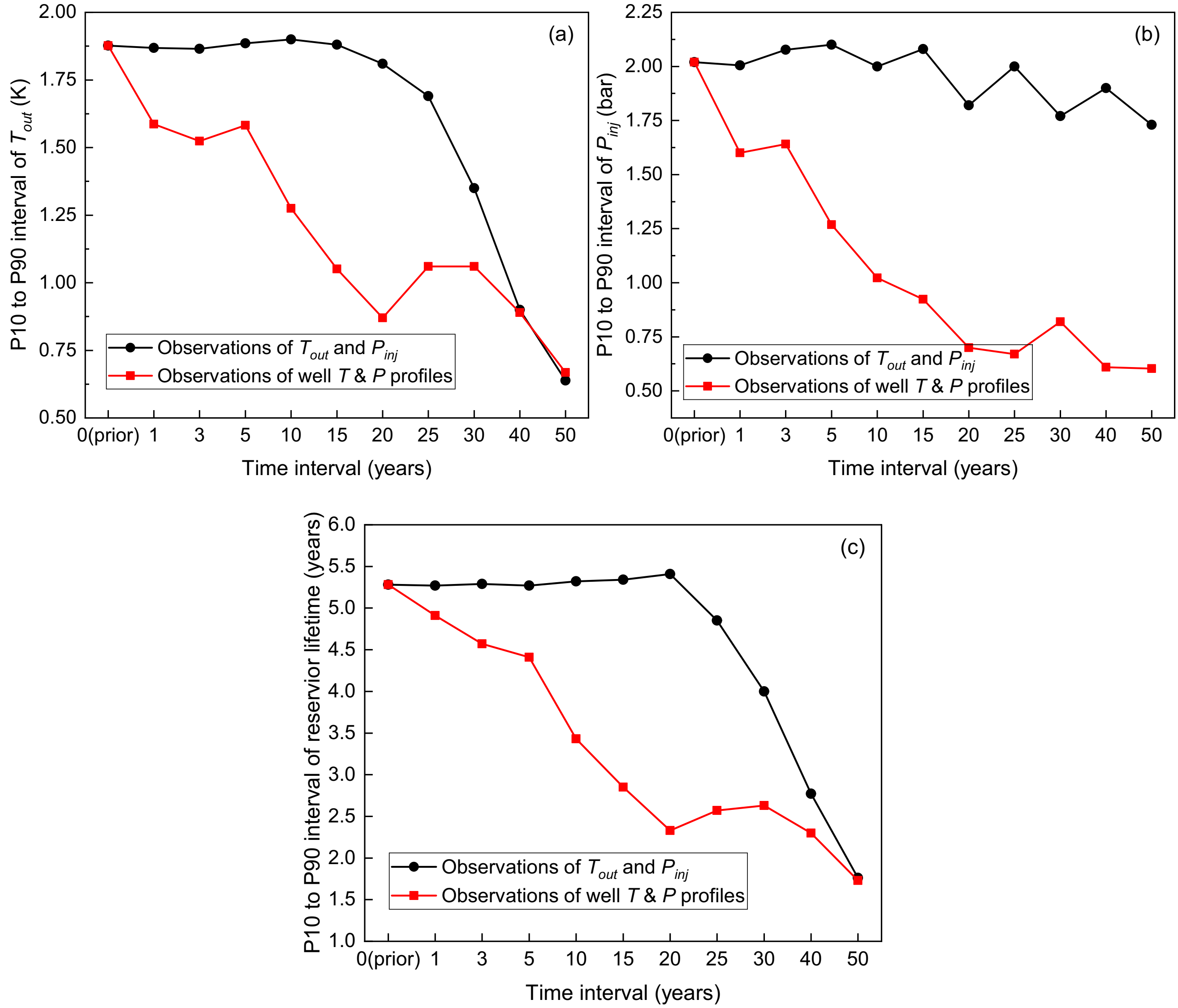


**Fig. 18** Variations in the P10 to P90 intervals for the production performance for different time intervals at which production data is observed in Cases # 15 (black) and #16 (red). The P10 to P90 intervals for production performance are quantified for $T_{out}$ after 50 years (**a**), $P_{inj}$ after 50 years (**b**) and the reservoir lifetime considering an abandonment temperature of 5 K below the initial $T_{out}$ (**c**)

occurs after approximately 20 years (Fig. 11). Hence there is little increase in information for any observations recorded at time intervals of less than 20 years since the start of production. However, such time scales for monitoring production data are likely already too late for operators to implement effective adjustments to avoid thermal breakthrough and extend the life-time of a geothermal system.

In contrast, when assimilating well temperature and pressure profiles in Case #16, the data worth increases consistently as the time interval for observing the production data increases (Fig. 17). The data worth increases even when only the data from the time interval of 1 year since the start of production is assimilated. Case #16 demonstrates a higher data worth than Case #15, indicating that the observations of well temperature and pressure profiles include significantly more informative data than $T_{out}$ and $P_{inj}$. Moreover, assimilating well profiles over increasing time intervals leads to a gradual reduction in the P10 to P90 intervals for $T_{out}$ and $P_{inj}$ after 50 years of production, as well as the prediction of the reservoir lifetime (Fig. 18). For the observation in 1-year time interval, the P10 to P90 intervals for $T_{out}$, $P_{inj}$ and reservoir lifetime is 1.59 K, 1.27 bar, and 4.41 years, representing reductions of 16%, 21%, and 7% compared to the prior production forecasts. Although the reduction is not substantial, it is still helpful as it could enable operators to design mitigation strategies early in the exploitation to enhance long-term reservoir performance and extend the geothermal system's lifetime.

## 3.4 Data-worth analysis considering different geological scenarios

For each scenario, the same observation data, i.e. temperature and pressure profiles along the injection well, production well, and monitoring borehole from the reference case are assimilated; this approach corresponds to the data acquisition strategy of Case #2. Although the posterior curves show a reduced P10 to P90 interval, there are notable deviation of both prior and posterior profiles from the reference data for Example #1 (Fig. 19) and Example #2 (Fig. 20). These deviations clearly show the impact of differences in channel distribution and geometry compared to the reference scenario on the resulting reservoir performance forcasts. In particular, the posterior profiles in Example #2 deviate more strongly from the reference than those in Example #1. The average posterior RMSEs along four virtual lines in example #2 are 15.53 K and 1.40 bar, which are substantially larger than the corresponding values of 5.62 K and 0.71 bar in Example #1. Although the RMSEs in both examples are higher than those of the reference scenario (1.46 K and 0.14 bar), the posterior results of Eaxmple #1 remain closer to the reference than Example #2. Therefore, Example #2 can be falsified.

The histograms of normalized *Tr* and RMSE for the ten different geological scenarios, i.e. reservoir architectures (Fig. 21), indicate that the average data worth of a data acquisition strategy corresponding to Case #2 is higher for scenarios where channel geometries are not constrained to any facies distributions. The posterior RMSE of temperature and pressure profiles observed along the wells is higher for geological scenarios without any facies constraints compared to geological scenarios where facies distributions are constrained using well data. This observation clearly demonstrates the need to consider multiple geological scenarios when modelling geothermal reservoirs and forecasting the reservoir performance.

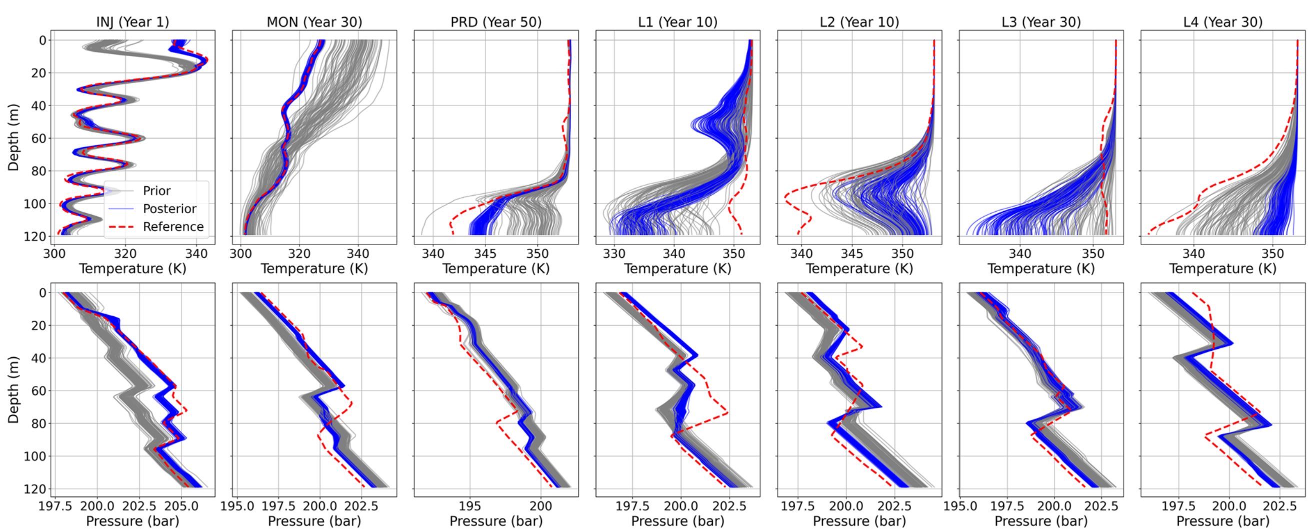


**Fig. 19** Prior, posterior, and reference temperature and pressure profiles recorded as a function of depth for the injection well (INJ), monitoring borehole (MON), production well (PRD) and four virtual lines (L1 to L4) at different times, respectively (from left to right) for Example #1. The data acquisition strategy is same as that in Case #2 where the temperature and pressure profiles along the injection well, production well, and monitoring borehole are observed. See Fig. 10 for the definitions of the colored lines

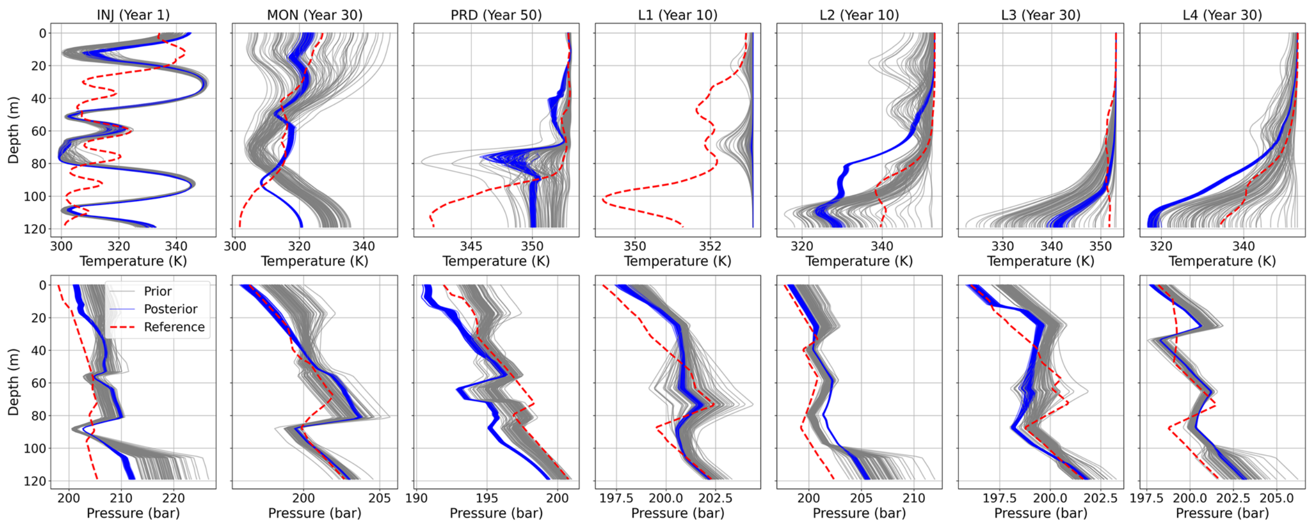


**Fig. 20** Prior, posterior, and reference temperature and pressure profiles recorded as a function of depth for the injection well (INJ), monitoring borehole (MON), production well (PRD) and four virtual lines (L1 to L4) at different times, respectively (from left to right) for Example #2. The data acquisition strategy is same as that in Case #2 where the temperature and pressure profiles along the injection well, production well, and monitoring borehole are observed. See Fig. 10 for the definitions of the colored lines

Recall that the RMSE evaluates the deviation of the simulated reservoir performance forecast from the observed reservoir performance, whereas normalized *Tr* evaluates the data worth of a data acquisition strategy. Hence any geological scenario where the simulation results yield a large RMSE should be falsified [42], as a large RMSE indicates that the reservoir architecture is likely inconsistent with the reservoir architecture present in the subsurface. In contrast, geological scenarios where the simulation results yield a lower RSME should be retained as they are likely to contain reservoir architectures that are more plausible, i.e. similar to the reservoir architectures present in the subsurface. In other words, data-worth analysis is more reliable when conducted for more plausible geological scenarios. That is, the data-worth evaluation of data-acquisition strategies can become unreliable if geological scenarios are considered where the reservoir architecture differs strongly from the actual reservoir geometry in the subsurface. Using the RMSE results for the posterior simulation results helps to falsify geological scenarios [42], allowing data-worth analysis to be performed for more plausible geological scenarios to ensure a more robust and reliable assessment of data acquisition strategies.

## 4 Discussion

Using ES-MDA, we are able to quantify data worth based on the difference between prior and posterior ensemble predictions. The uncertainty of predictions of interest is directly obtained from the ensemble members, which naturally accounts for correlations between parameters and observations. In contrast, sensitivity-based data-worth methods where data worth is derived from separate simulation results are generally suited to locally linear problems [8, 9]. Our geothermal production problem is inherently nonlinear: thermal breakthrough depends on the highly heterogeneous channel geometry, the connectivity of high-permeability zones, and strong couplings between pressure, temperature, and fluid properties (e.g., viscosity). Sensitivity analyses often neglect parameter correlations (e.g., the link between channel geometry and permeability) and redundancies in observation data (e.g., overlapping information from well pressure and temperature profiles as shown in Sect. 3.3.1). Our proposed ensemble-based approach captures the nonlinear features related to the reservoir dynamics, petrophysical property

 https://doi.org/10.1007/s10596-026-10460-3

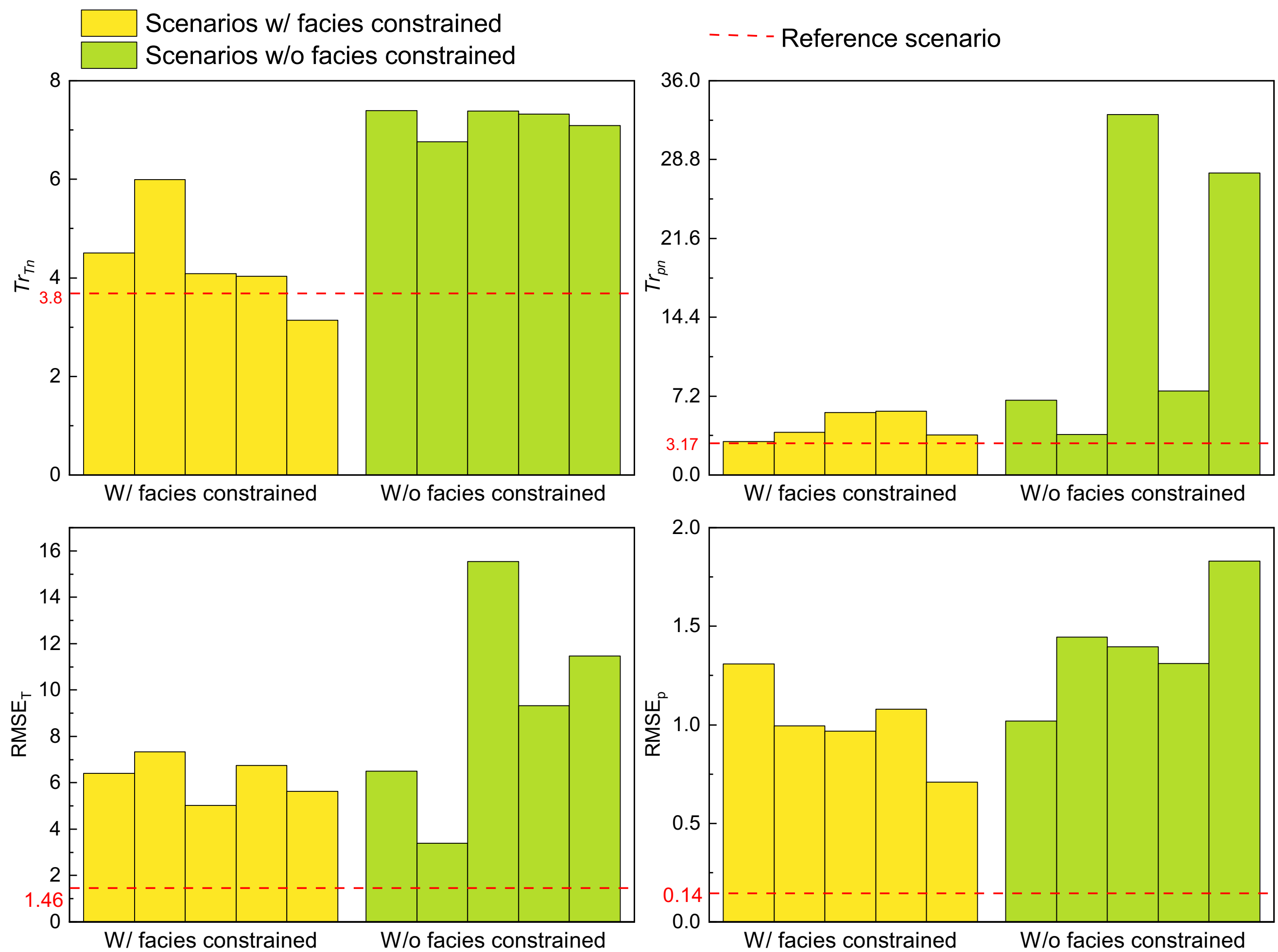


**Fig. 21** Histograms of normalized data worth and RMSE for the 10 different geological scenarios. The data-worth analysis is based on assimilating the temperature and pressure profiles along the injection well, production well, and monitoring borehole (Case #2). The RMSE is calculated from the posterior temperature and pressure profiles along the four virtual lines. All data worth values are normalized with respect to Case #1. Yellow bars represent five scenarios where channel geometries are constrained by facies distribution along the injector and producer while green bars represent five channel geometries without any facies constraints

distributions, and reservoir architecture. This capability is particularly important for geothermal systems located in geologically complex reservoirs such as channelized fluvial systems.

Preliminary uncertainty analysis can help identify the most uncertain reservoir properties as well as potential locations where reliable observation data could be recorded. Such knowledge can help geothermal operators to assess, for example, if placing fiber optics in wells is helpful in providing additional data that reduces uncertainties in reservoir performance forecasts and hence leads to more reliable reservoir management strategies that prolong the life time and increase the operational efficiency of a geothermal system.

Our findings are consistent with previous work that combines global sensitivity analysis and Bayesian data-worth analysis, which targets measurements in regions where simulation results indicate the highest parameter sensitivity [7, 13]. In the context of geothermal systems, the uncertainty in observed temperature profiles is directly related to the uncertainty in the advancement of the cold front. Cost-effective observation strategies that can constrain the advancement of the cold front could hence allow operators to reduce the overall uncertainty in forecasting the performance of a geothermal system. For example, geophysical techniques such as diffusive electromagnetic methods could potentially provide complementary information on the advancement of the cold front [28], yet most likely with substantial additional costs and lower resolution. If available, data from deviated boreholes in multi-well geothermal systems would also yield valuable information to reduce uncertainties in reservoir performance forecasts because deviated boreholes capture a larger portion of the cold front.

The data worth of observations in this study strongly depends on the timing of the thermal breakthrough. Transient data in the form of $T_{out}$ and $P_{inj}$ alone do not provide meaningful information until thermal breakthrough at the production well occurs. In contrast, early-time observations of temperature and pressure profiles recorded along wells, e.g. using fiber optics, provide increasingly more valuable information that gradually reduces the uncertainty in the production forecast. This is because thermal breakthrough emanates from the injector and the temperature profiles along the injection well capture this early migration of the cold front. Observational data in the form of temperature and pressure profiles along the well trajectories hence yield a higher information compared to $T_{out}$ and $P_{inj}$, especially at early times, and can help operators make timely decisions to improve the operation of a geothermal system. As a result, geological uncertainty can be propagated into economic uncertainty through probabilistic modeling frameworks [39, 53].

Our data-worth analysis for different geological scenarios, each representing a different reservoir architecture, shows that the data worth for a specific data acquisition strategy varies for different geological scenarios. Relying on a single geological scenario when performing a data-worth analysis hence can lead to an unreliable evaluation of the information of a data acquisition strategy. Using our previously proposed scenario-based data assimilation strategy that allows us to falsify geological scenarios based on RMSE results [42, 44] enables us to perform a data-worth analysis that considers different geological scenarios. This approach therefore helps us to analyze the effectiveness and reliability of different data-acquisition strategies across a broad range of geological uncertainties, i.e. reservoir architectures and petrophysical property distributions, which ultimately leads to more reliable reservoir performance forecasts.

However, several limitations in our proposed method need to be addressed. The most useful information for reducing uncertainties only emerges once thermal breakthrough has occurred. Yet, once breakthrough has occurred, no remedial actions can be taken, and the success or failure of a project is already evident. Ideally, reservoir architecture and the distribution of petrophysical properties should already be constrained long before thermal breakthrough, enabling operational adjustments to extend production life. The Delft campus geothermal project is also a rare exception in that a dedicated monitoring borehole will be drilled. Such a monitoring borehole will increase the value of data, improve data assimilation, and constrain uncertainties, it is unlikely that many direct-use geothermal systems will have such additional data available due to the high cost of drilling additional wells. Therefore, one should further explore the potential of using pressure transient data or geophysical monitoring methods that provide early-time data to improve the understanding of the reservoir architecture before thermal breakthrough occurs. In addition, a unified metric combining uncertainty and bias would provide a more comprehensive assessment of data worth, such as measures from information theory such as relative entropy (Kullback–Leibler divergence) [11], which account for both changes in variance and shifts in the mean of probability distributions. It should be noted that the data-worth calculation in this study is based on a single selected realization as the reference. As a result, the reported data-worth values are conditional on this choice and may vary if a different realization were used as the reference. A more comprehensive assessment would involve repeating the analysis using multiple realizations as alternative references to evaluate the robustness of the results.

## 5 Conclusions

This study proposes an ES-MDA-based data-worth analysis to quantify how different data acquisition strategies improve production forecasts and the understanding of reservoir dynamics in fluvial geothermal systems. By combining ES-MDA with heat and fluid-flow simulations in open-DARTS, we evaluated the data worth of different data acquisition strategies in terms of types of observed variables, number and locations of monitoring

https://doi.org/10.1007/s10596-026-10460-3

boreholes, configurations of monitoring boreholes, and time-scales of observation periods. Data-worth analysis is conducted across multiple geological scenarios, each representing different reservoir architectures. The main conclusions are:

1. ES-MDA-based data-worth analysis is an effective approach for assessing the value of data acquisition strategies in geothermal systems.
2. Incorporating production temperature and injection pressure reduces uncertainty of production forecasts but is insufficient to constrain reservoir dynamics. Adding temperature and pressure profiles recorded along wells (e.g., using fiber optics) significantly improves the reliability of reservoir performance forecasts and our understanding of the reservoir dynamics.
3. Under constant-rate injection condition for a geothermal doublet system, temperature profiles recorded along wells provide higher data worth than pressure profiles recorded along the same well. A deviated monitoring borehole also provides more information than a vertical monitoring borehole. Importantly, temperature and pressure profiles recorded along wells provide valuable information during the early stage of production that enables timely reservoir management decisions to adjust operations before thermal breakthrough occurs.
4. Data-worth analysis should always be performed across multiple geological scenarios. Geological scenarios with high RMSE for the simulation results can be falsified, while scenarios with lower RMSE can be retained as they likely contain reservoir architectures that are plausible, i.e. more representative of the real reservoir architecture that is present in the subsurface yet unknown. Conducting data-worth analysis across multiple plausible geological scenarios is key to ensuring that a reliable data acquisition strategy can be designed that helps to reduce uncertainties in the reservoir performance forecasts well before thermal breakthrough occurs.

**Acknowledgements** We thank the anonymous reviewers and editors for their insightful comments which have helped to improve the original manuscript.

**Author contributions** G.S.: Data Curation, Investigation, Formal Analysis, Methodology, Writing – Original Draft. D.V.: Software, Methodology, Writing – Review & Editing. H.A.: Resources, Writing – Review & Editing. P.V.: Project Administration, Writing – Review & Editing. S.G.: Conceptualization, Resources, Funding Acquisition, Supervision, Writing – Review & Editing, Project Administration.

**Funding** This research was supported by the TU Delft Excellence Foundation and the Energi Simulation Chair of Sebastian Geiger.

**Data availability** The data that support the findings of this study are available from the corresponding author upon reasonable request.

## Declarations

**Competing interests** The authors declare no competing interests.

## References

1. Witter, J.B., Trainor-Guitton, W.J., Siler, D.L.: Uncertainty and risk evaluation during the exploration stage of geothermal development: a review. Geothermics **78**, 233–242 (2019). https://doi.org/10.1016/j.geothermics.2018.12.011
2. Ringrose, P., Bentley, M.: Reservoir model design. Springer (2016)
3. Song, G., Geiger, S., Voskov, D., Abels, H., Vardon, P.: Data worth analysis for a fluvial geothermal system using an ensemble smoother with multiple data assimilation. Sixth EAGE Global Energy Transition Conference & Exhibition (GET 2025) **2025**(1), 1–5 (2025). https://doi.org/10.3997/2214-4609.202521048
4. Neuman, S.P., Xue, L., Ye, M., Lu, D.: Bayesian analysis of data-worth considering model and parameter uncertainties. Adv. Water Resour. **36**, 75–85 (2012). https://doi.org/10.1016/j.advwatres.2011.02.007
5. Gosses, M., Wohling, T.: Robust data worth analysis with surrogate models. Ground Water **59**(5), 728–744 (2021). https://doi.org/10.1111/gwat.13098
6. Wang, Y.K., Shi, L.S., Lin, L., Holzman, M., Carmona, F., Zhang, Q.R.: A robust data-worth analysis framework for soil moisture flow by hybridizing sequential data assimilation and machine learning. Vadose Zone J. **19**(1), e20026 (2020). https://doi.org/10.1002/vzj2.20026
7. Dausman, A.M., Doherty, J., Langevin, C.D., Sukop, M.C.: Quantifying data worth toward reducing predictive uncertainty. Ground Water **48**(5), 729–740 (2010). https://doi.org/10.1111/j.1745-6584.2010.00679.x
8. Finsterle, S.: Practical notes on local data-worth analysis. Water Resour. Res. **51**(12), 9904–9924 (2015). https://doi.org/10.1002/2015wr017445
9. Finsterle, S., Kober, F., Vomvoris, S., Lanyon, B., Kowalsky, M.: Data-worth analysis for the design of the HotBENT monitoring system. Geoenergy **1**(1), geoenergy2023-020 (2023). https://doi.org/10.1144/geoenergy2023-020
10. Wang, Y.K., Shi, L.S., Zha, Y.Y., Li, X.M., Zhang, Q.R., Ye, M.: Sequential data-worth analysis coupled with ensemble Kalman filter for soil water flow: A real-world case study. J. Hydrol. **564**, 76–88 (2018). https://doi.org/10.1016/j.jhydrol.2018.06.059
11. Wang, Y.K., Hu, X.L., Wang, L.J., Li, J.M., Lin, L., Huang, K., Shi, L.S.: Data worth analysis within a model-free data assimilation framework for soil moisture flow. Hydrol. Earth Syst. Sci. **27**(14), 2661–2680 (2023). https://doi.org/10.5194/hess-27-2661-2023
12. Xue, L., Zhang, D.X., Guadagnini, A., Neuman, S.P.: Multimodel Bayesian analysis of groundwater data worth. Water Resour. Res. **50**(11), 8481–8496 (2014). https://doi.org/10.1002/2014wr015503
13. Younes, A., Shao, Q., Mara, T.A., Baalousha, H.M., Fahs, M.: Use of global sensitivity and data-worth analysis for an efficient estimation of soil hydraulic properties. Water **12**(3), 736 (2020). https://doi.org/10.3390/w12030736
14. Dai, C., Xue, L., Zhang, D.X., Guadagnini, A.: Data-worth analysis through probabilistic collocation-based ensemble Kalman filter. J. Hydrol. **540**, 488–503 (2016). https://doi.org/10.1016/j.jhydrol.2016.06.037
15. Xue, L.: Application of the multimodel ensemble Kalman filter method in groundwater system. Water **7**(2), 528–545 (2015). https://doi.org/10.3390/w7020528
16. Zhan, C.J., Dai, Z.X., Soltanian, M.R., Zhang, X.Y.: Stage-wise stochastic deep learning inversion framework for subsurface sedimentary structure identification. Geophys. Res. Lett. **49**(1), e2021GL095823 (2022). https://doi.org/10.1029/2021GL095823
17. Song, G., Roubinet, D., Wang, X., Li, G., Song, X., Tartakovsky, D.M.: Surrogate models of heat transfer in fractured rock and their use in parameter estimation. Comput. Geosci. **183**, 105509 (2024). https://doi.org/10.1016/j.cageo.2023.105509
18. Athens, N.D., Caers, J.K.: A Monte Carlo-based framework for assessing the value of information and development risk in geothermal exploration. Appl. Energy **256**, 113932 (2019). https://doi.org/10.1016/j.apenergy.2019.113932
19. Zhan, C.J., Dai, Z.X., Soltanian, M.R., de Barros, F.P.J.: Data-worth analysis for heterogeneous subsurface structure identification with a stochastic deep learning framework. Water Resour. Res. **58**(11), e2022WR033241 (2022). https://doi.org/10.1029/2022WR033241
20. Eidsvik, J., Mukerji, T., Bhattacharjya, D.: Value of information in the earth sciences: integrating spatial modeling and decision analysis. Cambridge University Press (2015)
21. GD Barros, E., Van den Hof, P., Jansen, J.: Value of information in closed-loop reservoir management. Comput. Geosci. **20**(3), 737–749 (2016). https://doi.org/10.1007/s10596-015-9509-4
22. Barros, E., Leeuwenburgh, O., Szklarz, S.: Quantitative assessment of monitoring strategies for conformance verification of CO2 storage projects. Int. J. Greenhouse Gas Control **110**, 103403 (2021). https://doi.org/10.1016/j.ijggc.2021.103403
23. van Wees, J.D., Veldkamp, H., Brunner, L., Vrijlandt, M., de Jong, S., Heijnen, N., van Langen, C., Peijster, J.: Accelerating geothermal development with a play-based portfolio approach. Neth. J. Geosci. **99**, e5 (2020). https://doi.org/10.1017/njg.2020.4
24. Van Unen, M., Brunner, L., Veldkamp, H., Keijzer, R., Van Wees, J. D.: De-risking of geothermal prospect portfolios based on Value of Information and a play-based exploration approach: a case study for Slochteren reservoir development in the Netherlands. Glob. Planet Change. 105130 (2025). https://doi.org/10.1016/j.gloplacha.2025.105130

25. Seabra, G.S., Mücke, N.T., Silva, V.L.S., Voskov, D., Vossepoel, F.C.: AI enhanced data assimilation and uncertainty quantification applied to Geological Carbon Storage. Int. J. Greenhouse Gas Control **136**, 104190 (2024). https://doi.org/10.1016/j.ijggc.2024.104190
26. Emerick, A.A., Reynolds, A.C.: Ensemble smoother with multiple data assimilation. Comput. Geosci. **55**, 3–15 (2013). https://doi.org/10.1016/j.cageo.2012.03.011
27. Wu, H., Fu, P.C., Hawkins, A.J., Tang, H.W., Morris, J.P.: Predicting thermal performance of an enhanced geothermal system from tracer tests in a data assimilation framework. Water Resour. Res. **57**(12), e2021WR030987 (2021). https://doi.org/10.1029/2021WR030987
28. Oudshoorn, C., Werthmüller, D., Slob, E., Voskov, D.: Numerical experiment on data assimilation for geothermal doublets using production data and electromagnetic observations. Geophysics **89**(6), M227–M237 (2024). https://doi.org/10.1190/Geo2023-0463.1
29. Song, G., Geiger, S., Voskov, D., Abels, H. A., Vardon, P. J.: Assessing the ensemble smoother with multiple data assimilation for subsurface fluvial geothermal systems. 50th Workshop Geotherm. Reservoir Eng. (2025).
30. Evensen, G., Vossepoel, F.C., Van Leeuwen, P.J.: Data assimilation fundamentals: a unified formulation of the state and parameter estimation problem. Springer Nature (2022)
31. Larue, D.K., Hovadik, J.: Connectivity of channelized reservoirs: a modelling approach. Pet. Geosci. **12**(4), 291–308 (2006). https://doi.org/10.1144/1354-079306-699
32. Villamizar, C.A., Hampson, G.J., Flood, Y.S., Fitch, P.J.R.: Object-based modelling of avulsion-generated sandbody distributions and connectivity in a fluvial reservoir analogue of low to moderate net-to-gross ratio. Pet. Geosci. **21**(4), 249–270 (2015). https://doi.org/10.1144/petgeo2015-004
33. Choi, K., Jackson, M.D., Hampson, G.J., Jones, A.D.W., Reynolds, A.D.: Predicting the impact of sedimentological heterogeneity on gas-oil and water-oil displacements: fluvio-deltaic Pereriv Suite Reservoir, Azeri-Chirag-Gunashli Oilfield. South Caspian Basin. Petroleum Geoscience **17**(2), 143–163 (2011). https://doi.org/10.1144/1354-079310-013
34. Bentley, M., Smith, S.: Scenario-based reservoir modelling: the need for more determinism and less anchoring. Futur. Geol. Model. Hydrocarbon Dev. **309**(1), 145–159 (2008). https://doi.org/10.1144/Sp309.11
35. Aghaei, H., Colombera, L., Yan, N., Mountney, N. P., Bernagozzi, G., Di Giulio, A.: Impact of fluvial meander-belt sedimentary heterogeneity on the efficiency of low-enthalpy geothermal doublets: heat-transport simulations of forward stratigraphic models. Geoenergy, Geoenergy2024-024 (2024). https://doi.org/10.1144/geoenergy2024-024
36. Vardon, P., Abels, H., Barnhoorn, A., Daniilidis, A., Bruhn, D., Drijkoningen, G., Elliott, K., van Esser, B., Laumann, S., van Paassen, P.: A research and energy production geothermal project on the TU Delft campus: Project implementation and initial data collection. 49th Workshop on Geothermal Reservoir Engineering, (2024).
37. Voskov, D., Abels, H., Barnhoorn, A., Chen, Y., Daniilidis, A., Bruhn, D., Drijkoningen, G., Geiger, S., Laumann, S., Song, G.: A research and production geothermal project on the TU Delft campus: initial modeling and establishment of a digital twin. 49th Workshop Geotherm. Reservoir Eng. (2024).
38. Willems, C.J.L., Vondrak, A., Mijnlieff, H.F., Donselaar, M.E., van Kempen, B.M.M.: Geology of the Upper Jurassic to Lower Cretaceous geothermal aquifers in the West Netherlands Basin - an overview. Netherlands J. Geosci.-Geol. En Mijnbouw **99**, e1 (2020). https://doi.org/10.1017/njg.2020.1
39. Wang, Y., Voskov, D., Daniilidis, A., Khait, M., Saeid, S., Bruhn, D.: Uncertainty quantification in a heterogeneous fluvial sandstone reservoir using GPU-based Monte Carlo simulation. Geothermics **114**, 102773 (2023). https://doi.org/10.1016/j.geothermics.2023.102773
40. Chen, Y., Voskov, D., Daniilidis, A.: Rigorous numerical methodology and heat recovery analysis for modeling of direct use geothermal systems. Geoenergy Sci. Eng. **247**, 213661 (2025). https://doi.org/10.1016/j.geoen.2025.213661
41. Daniilidis, A.: Towards comprehensive uncertainty quantification in direct-use geothermal systems. 85th EAGE Annu. Conf. Exhibition. **2024**(1), 1-5 (2024). https://doi.org/10.3997/2214-4609.2024101678
42. Song, G., Geiger, S., Voskov, D., Abels, H. A., Vardon, P. J.: Scenario-based data assimilation framework to improve production estimates for geologically complex geothermal reservoirs. Geoenergy Sci. Eng. **263**, 214490 (2026). https://doi.org/10.1016/j.geoen.2026.214490
43. Jacquemyn, C., Pataki, M.E.H., Hampson, G.J., Jackson, M.D., Petrovskyy, D., Geiger, S., Marques, C.C., Silva, J.M.D., Judice, S., Rahman, F., Sousa, M.C.: Sketch-based interface and modelling of stratigraphy and structure in three dimensions. J. Geol. Soc. **178**(4), jgs2020-187 (2021). https://doi.org/10.1144/jgs2020-187
44. Song, G., Geiger, S., Abels, H., Voskov, D., Vardon, P., Jackson, M., Hampson, G., Jacquemyn, C., Petrovskyy, D.: Towards a subsurface geothermal digital twin: efficient construction of geological scenarios for modelling fluvial geothermal reservoirs. Fifth EAGE Glob. Energy Transit. Conf. Exhibition (GET 2024) **2024**(1), 1–5 (2024). https://doi.org/10.3997/2214-4609.202421162
45. Khait, M., Voskov, D.: Operator-based linearization for efficient modeling of geothermal processes. Geothermics **74**, 7–18 (2018). https://doi.org/10.1016/j.geothermics.2018.01.012
46. Nowak, M., Verly, G.: The practice of sequential gaussian simulation. Springer (2004)
47. Bai, T., Tahmasebi, P.: Sequential Gaussian simulation for geosystems modeling: A machine learning approach. Geosci. Front. **13**(1), 101258 (2022). https://doi.org/10.1016/j.gsf.2021.101258

48. Khait, M., Voskov, D.V.: Operator-based linearization for general purpose reservoir simulation. J. Petrol. Sci. Eng. **157**, 990–998 (2017). https://doi.org/10.1016/j.petrol.2017.08.009
49. Wang, Y., Voskov, D., Khait, M., Bruhn, D.: An efficient numerical simulator for geothermal simulation: A benchmark study. Appl. Energy **264**, 114693 (2020). https://doi.org/10.1016/j.apenergy.2020.114693
50. Wang, Y., Voskov, D., Khait, M., Saeid, S., Bruhn, D.: Influential factors on the development of a low-enthalpy geothermal reservoir: a sensitivity study of a realistic field. Renew. Energy **179**, 641–651 (2021). https://doi.org/10.1016/j.renene.2021.07.017
51. Le, D.H., Reynolds, A.C.: Estimation of mutual information and conditional entropy for surveillance optimization. SPE J. **19**(04), 648–661 (2014). https://doi.org/10.2118/163638-PA
52. Le, D.H., Reynolds, A.C.: Optimal choice of a surveillance operation using information theory. Comput. Geosci. **18**(3), 505–518 (2014). https://doi.org/10.1007/s10596-014-9401-7
53. Ezekiel, J., Ebigbo, A., Arifianto, I., Daniilidis, A., Finkbeiner, T., Mai, P.M.: Techno-economic performance optimization of hydrothermal doublet systems: Application to the Al Wajh basin, Western Saudi Arabia. Geothermics **105**, 102532 (2022). https://doi.org/10.1016/j.geothermics.2022.102532




## Authors and Affiliations


**Guofeng Song[1] · Denis Voskov[1,2] · Hemmo A. Abels[1] · Philip J. Vardon[1] · Sebastian Geiger[1]**

✉ Guofeng Song
G.Song-1@tudelft.nl

[1] Department of Geoscience & Engineering, Delft University of Technology, Delft, The Netherlands

[2] Department of Energy Science & Engineering, Stanford University, Stanford, CA, USA